

Review

Carbon Sphere Template Derived Hollow Nanostructure for Photocatalysis and Gas Sensing

Zirui Lou, Yichen Wang, Yingchen Yang, Yanwen Wang, Chao Qin, Rong Liang, Xuehua Chen, Zhizhen Ye and Liping Zhu * 

State Key Laboratory of Silicon Materials, School of Materials Science & Engineering, Zhejiang University, Hangzhou 310027, China; zrlou@zju.edu.cn (Z.L.); pifuwuze@zju.edu.cn (Y.W.); ycyang@zju.edu.cn (Y.Y.); 21826067@zju.edu.cn (Y.W.); 21626044@zju.edu.cn (C.Q.); liangr@zju.edu.cn (R.L.); threed_cxh@zju.edu.cn (X.C.); yezz@zju.edu.cn (Z.Y.)

* Correspondence: zlp1@zju.edu.cn

Received: 12 January 2020; Accepted: 17 February 2020; Published: 21 February 2020



Abstract: As a green and preferred technology for energy crisis and environmental issues, continuous research on photocatalysis and gas sensing has come forth at an explosive rate. Thus far, promising synthetic methods have enabled various designs and preparations of semiconductor-based nanostructure which have shown superior activity. This review summarized various synthetic routines toward carbon sphere template derived hollow nanostructures and their successful attempts in synthesize doping, solid solution, heterostructure, and surface modified nanostructures for heterogeneous photocatalysis and gas sensing. Moreover, the challenges and future prospects are briefly discussed. It is eagerly anticipated that this review may broaden the view and in-depth understanding of carbon sphere template derived hollow nanostructures while expected to have further progresses in heterogeneous photocatalysis, gas sensing and other related fields which will make great contributions to their application.

Keywords: carbon sphere; hollow structure; doping; solid solution; heterostructure; surface modification

1. Introduction

Developing sustainable energy is one of the most urgent tasks of humankind. With the development of science and technology, the explosive growth of energy demand is making limited traditional fossil energy stretched thin. Among various types of sustainable energy, solar energy is the most abundant renewable energy source on earth. However, it is dilute, unequally distributed, and intermittent. Hence, to harness solar energy facilely, efficiently and economically remains a challenge [1]. Solar driven photocatalysis based on particulate photocatalysts is a potentially scale-up industrial and economically practical technology to convert solar energy into chemical energy. Since 1972, when Fujishima and Honda first reported the phenomenon of hydrogen generation from the decomposition of water by TiO₂ photocatalysts, photocatalysis has gradually attracted the attention of academia and industry [2]. In 2001, Zou et al. [3] first discovered In_{1-x}Ni_xTaO₄ photocatalyst with visible light activity for photolytic water splitting. The past two decades, various kinds of semiconductor photocatalysts have been widely studied, such as oxides [4–9], sulfides [10–14], nitrides [15–18], carbides [15,19–21], etc. Domen's recent studies based on particulate photocatalyst sheets provide a possible way for the large-scale and practical photocatalytic water splitting [22–24].

A typical photocatalytic process mainly consists of three steps: (i) semiconductors absorb light of corresponding wavelength with appropriate bandgap; (ii) transition of photo induced carriers from valence band to conduction band; (iii) carrier migration to material surface for redox reaction

with reactants [25]. However, the band gaps of most metal oxides are too large to avail adequate absorption of the majority of photons in the solar spectrum [26]. There are limitations in most semiconductor photocatalysts like fast charge carriers recombination, surface carrier recombination, as well as surface state pinning which prevent photogenerated carriers from participating in redox reaction [25]. In the study of particle photocatalysts, however, photocatalytic quantum efficiency of the bulk photocatalysts is limited by carrier migration, trapping, and recombination inside the bulks which account for most of the volume [27]. The nano form photocatalysts, with dimensions reaching tens of nanometers in scale, or even less than their corresponding Bohr radii, ought to possess enhanced photocatalytic quantum efficiency [28]. On account of the higher specific surface area and the smaller grain size, more surface catalytic sites and shorter distances from interior to surface of the material enable photo induced carriers to participate in surface redox reaction instead of loss in bulks. Similarly, designing and constructing nanostructures is the trend of enhancing sensing performance of semiconductor-based gas sensors.

To this end, researchers have synthesized nanomaterials by various methods and improved the efficiency of solar absorption and conversion efficiency of the photocatalysts by doping, constructing heterostructures and surface modification. Among them, carbon sphere template derived hollow nanostructure is one of the most promising methods to prepare high-efficiency photocatalysts and gas sensors due to some unique characteristics. First of all, the raw materials (any of the saccharides and some biomass) and products of template (carbon sphere) are environmentally friendly. Then, the surface functional groups adsorb metal ions uniformly and non-selectively, so we can realize doping, solid-solution, heterostructure, and surface modification easily by simply adjust the adsorption or annealing conditions. In view of these facts, we introduce a synthetic method that synthesizes a variety of multiple metal compound hollow spheres by using ions adsorption and templating approaches. This strategy could avoid the bulk form of the multiple metal compound in traditional synthesis process and tune the composition of different metals precisely. These multiple metal compound hollow spheres have shells in nanoscale and high specific surface areas, which bound to be helpful for photocatalysis, gas sensing, and other related reactions.

In this review, we will first give an overview on the synthesis of carbon sphere template and then summarized various synthetic routines toward carbon sphere template derived hollow nanostructures, including their advantages in synthesizing different types of nanostructure for photocatalysis (doping, solid-solution, heterostructure, surface modification). Secondly, their valuable applications in gas sensing using the same idea as photocatalyst modification will be summarized and discussed. At the end of this review, challenges and outlooks in the field of carbon sphere template derived hollow nanostructure are highlighted.

2. Carbon Sphere Template—Overview of Synthesis

Carbon spheres have been widely researched and applied to various fields—including batteries, photocatalysis, capacitors, and fuel cells—due to their easily available sources and facile synthesis. The last few decades have witnessed a rapid growth in sustainable energy field and this has led to the research of various application and approaches of carbon spheres, including carbonization routes [29], chemical vapor deposition (CVD) [30], ultrasonic-spray [31], and hydrothermal carbonization (HTC) [6,32,33]. Among these methods, hydrothermal carbonization is the one that aroused the greatest interest due to its facile procedure and mild experimental condition. Besides, carbon spheres obtained through HTC method have tunable diameters, great monodispersity, and excellent surface activities compared to carbon spheres synthesized by other procedures. Accordingly, HTC method is considered a perfect way to obtain carbon spheres as templates and assist the subsequent modification.

Wang et al. [34] successfully synthesized a novel monodispersed hard carbon spheres which is perfectly round with good surface condition and evenly distributed nanopores. In this experiment, carbon spheres were facilely prepared by two steps, including dehydration at low temperatures and

carbonization at high temperatures of glucose. Sun et al. [32] put forward a simplified hydrothermal procedure to synthesize micro- or nanospheres. Carbon nano- and microspheres were synthesized directly using aqueous glucose solution as precursor by the method of hydrothermal synthesis at 160–180 °C. The growth model of carbon spheres is shown schematically in Figure 1. The synthesis process is facile, and the as-prepared hard carbon spheres were tunable in diameters, crystallinity, chemical composition, with reactive surface and inherited functional groups of the precursor. Titirici et al. [35] reported a one-pot synthesis to obtain hollow spherical metal oxides such as Fe_2O_3 , Ni_2O_3 , Co_3O_4 , CeO_2 , MgO , and CuO via a hydrothermal approach by directly adding glucose or sucrose as precursor and metal oxide precursors. It is to be observed that, during the synthesis procedure, the carbon spheres were also formed and serve as templates and this method is more simplified but it has no harmful effects for metal oxide hollow spheres. Although the hydrothermal carbonization (HTC) method for carbon spheres is mature and widely used, there exist some limitations that restrict the formation of relatively small size of carbon sphere. Tan et al. [36] finally overcome this barrier by varying parameters of hydrothermal carbonization process—including glucose concentration, pH value, and temperature—and synthesize small-sized carbon spheres (40 nm) for the first time.

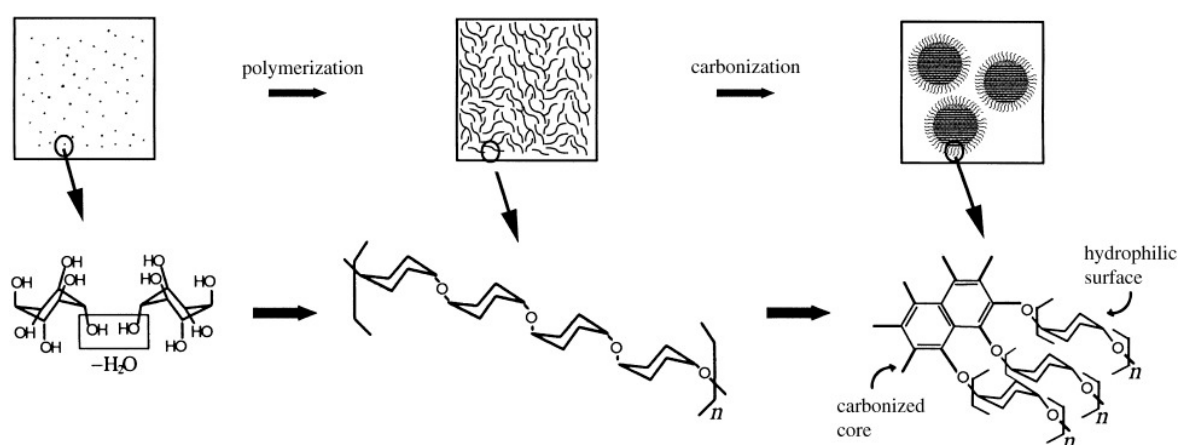


Figure 1. Schematics of the possible synthesis procedure of carbon spheres. Reproduced with permission from [32]. Copyright WILEY, 2004.

A typical hydrothermal synthesis for carbon sphere template consists of 5g glucose dissolving in 30 ml water, sealing in a 50 mL autoclave and maintaining at 180 °C for 6 h. The as-prepared templates were isolated by several rinsing-centrifugation cycles until the solution is clear and oven-dried. Among some details of the experiment, we found the dispersion of the template can be controlled by trace amount of surfactant, solubility of glucose and quenching of the autoclave.

Besides, surface property of carbon spheres and precursors of carbon spheres have been widely studied in recent years. The surface of carbon spheres, especially those synthesized from hydrothermal reaction, possess high density of hydrophilic groups such as $-\text{OH}$ and $\text{C}=\text{O}$ groups, so that can absorb various of metal ions easily and uniformly without any further modification [37]. This is the critical superiority when carbon spheres are applied as templates. Moreover, many researchers are focusing on a wide range of source to obtain carbon spheres by hydrothermal reaction, including general monosaccharide (xylose [38], glucose [38]), disaccharides (sucrose [6,38], lactose [39]), polysaccharides (starch [40,41], cellulose [42]), and some biomasses [39]. The possible formation procedure is shown schematically in Figure 2. These studies showed that all these sources could be applied to synthesize sphere-like carbon sphere-like structures which contained amounts of hydrophilic reactive functional group on the surface, but the qualities (such as morphology and dispersivity) of carbon spheres are better when saccharides are chosen as precursors due to the structural complexity of biomasses [39]. Despite all of this, using biomasses to synthesize carbon spheres will continue to be a hot spot because of its abundant resources, environmental friendliness, and consistency of sustainable development.

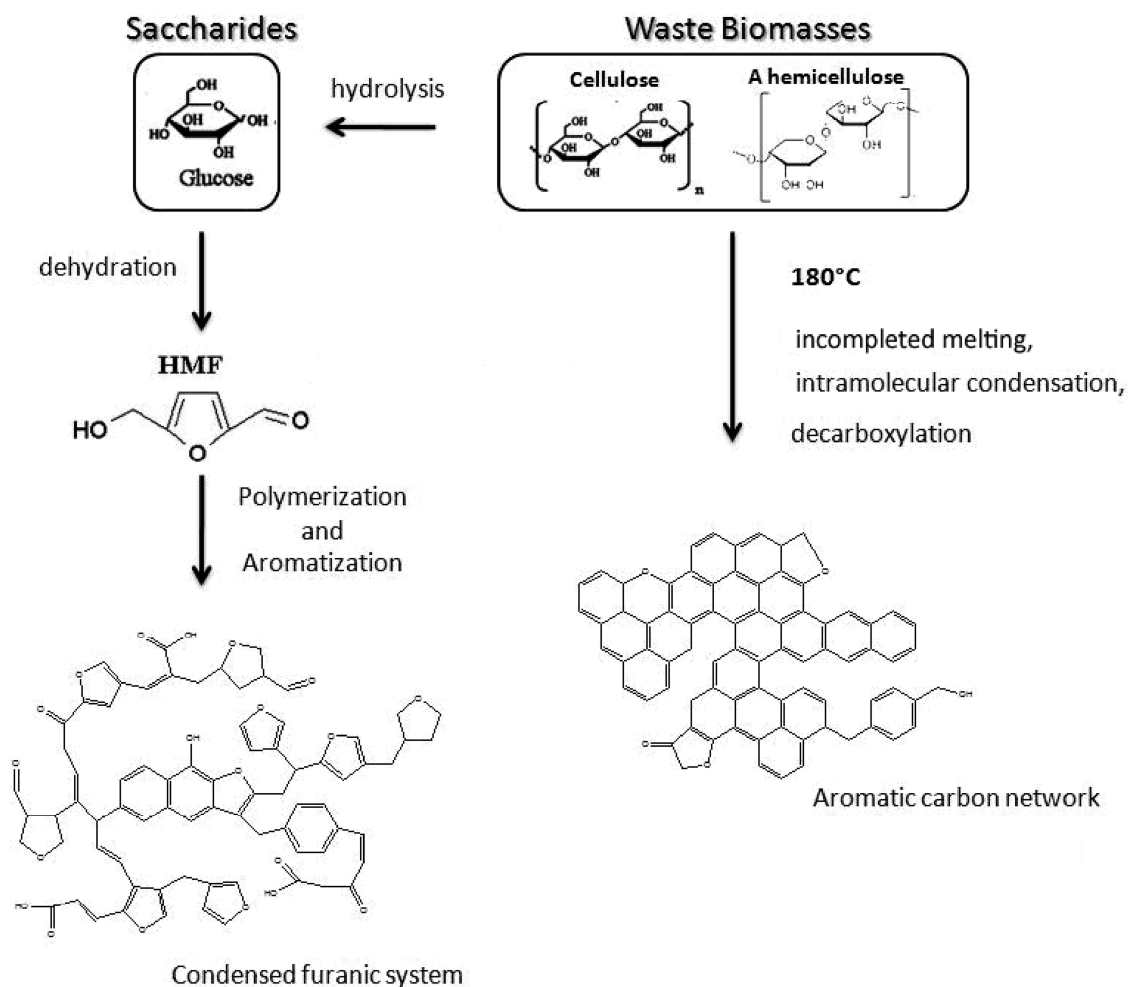


Figure 2. Proposed formation mechanism of sphere-like carbon synthesized from saccharides and biomasses. Reproduced with permission from [39]. Copyright American Chemical Society, 2012.

In addition, there are also some reports about sphere-like carbon with some changes of morphology, including mesoporous carbon, hollow carbon spheres, which can also be applied as templates [43–45]. Mesoporous and hollow carbon spheres are synthesized by a numerous methods, such as carbonization and a template procedure. Mesoporous hollow carbon spheres could be obtained through carbonization of polystyrene (PS) [43]. Carbon hollow spheres with tunable diameter and surface properties have studied and prepared with the use of templates such as silica spheres, some polymer spheres, metallic templates [44], and some other core templates [45]. There is still great necessity to deeply research the preparation of various carbon spheres (both morphology and property) to realize a synthesis method that starts with environmental-friendly materials and involves a facile synthesis process.

3. Carbon Sphere Template Derived Hollow Nanostructure: Advantages in Synthesizing Different Types of Nanostructures for Photocatalysis

From recent studies, the nanoscale morphology could conducive to enhance the charge carriers' separation and transfer efficiency as well as raise the density of catalytic sites and it is one of the keys to improve photocatalytic performances [27,28,37]. However, for these traditional methods such as sol-gel and sintering methods, a precipitation or solid-state reaction process is essential to mix the different metal ions on molecular level. Resultantly, the large particle size and the aggregation phenomena are inevitable in multiple metal compounds [46]. Thus a general method for the synthesis of multiple metal compounds consists of doping, heterostructure, and surface modification strategies in nanoscale is essential in photocatalysis. Carbon sphere template derived hollow nanostructure is

such a way to achieve the above strategies. Even controllable multi-layer hollow structures can be realized by different post-processing methods [47]. As shown in Figure 3, it is the illustration of carbon sphere template derived hollow nanoheterostructure and controllable multilayer structure.

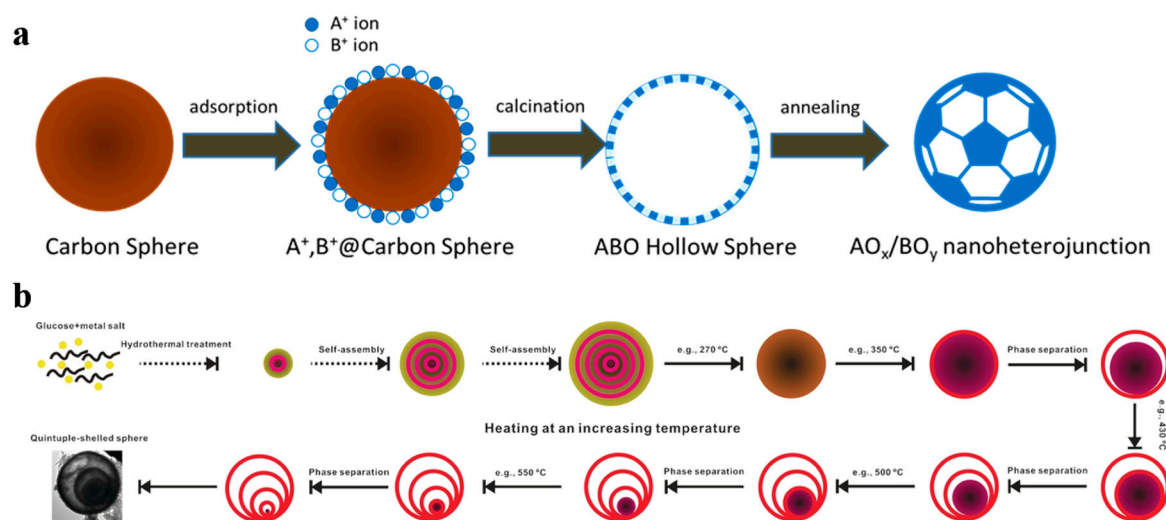


Figure 3. General process for the formation of carbon sphere template derived (a) hollow nanoheterostructure and (b) controllable multilayer structure. Reproduced with permission from [47]. Copyright WILEY, 2016.

3.1. Doping

Most metal oxide semiconductors with wide band gap could hardly respond to the visible light region [48], which limit their application in photocatalysis. Hence it is urgent to design semiconductor-based photocatalysts active both in UV and visible light region. Doping metal oxides (TiO₂, ZnO, WO₃, etc.), polymetallic oxides and nitrides [49] with non-metals (C, O, S, N, P, etc.) [48] or metals (Na, Mg, Fe, Lanthanide, etc.) [50] expand the effective absorption to visible light region to promote light harvesting and photocatalytic performance. One of many valid methods to design efficient photocatalysts which also can absorb visible light is creating impurity levels in band gap by doping [51]. We can achieve doping of many kinds of desired metals into oxides taking the characteristics of good dispersion of carbon sphere template and its uniformly and non-selectively adsorption of metal ions. By further regulating the experimental process, the doping of non-metallic elements can also be realized.

For instance, Song et al. [52] demonstrated that Fe doped contents can be precisely regulated by using this simple templating method, so that they acquired broader light absorption region. Fe doping introduced impurity levels in the forbidden band confirmed by DFT (density functional theory) calculation, which narrowed the band gap of WO₃. Meanwhile, WO₃ nanostructured photocatalysts with 5 at % Fe showed the best photocatalytic performance due to the low recombination and high transformation of the photo-generated carriers. Besides, Na-doped ZnO nanostructures have been firstly fabricated by ion adsorption and template method utilizing carbon spheres as templates [53]. Na and Zn elements cannot be precipitated simultaneously because their chemical activities in solution differ from each other. Instead of co-precipitation method, they gather the Zn and Na cations uniformly and simultaneously on the surface of carbon spheres (Figure 4a). Engineering the Zn-doped contents can tune the work function of Na-doped ZnO from 4.48 eV to 6.19 eV, and fermi level get closer to the level of valence band by the increasing of Na doping concentration, which presented the success of a *p*-type doping effect (Figure 4b). They have got Na-ZnO/Pt with 0.7 at % which presented the highest photocatalytic H₂ generation rate and it was obviously superior to pure ZnO (Figure 4c).

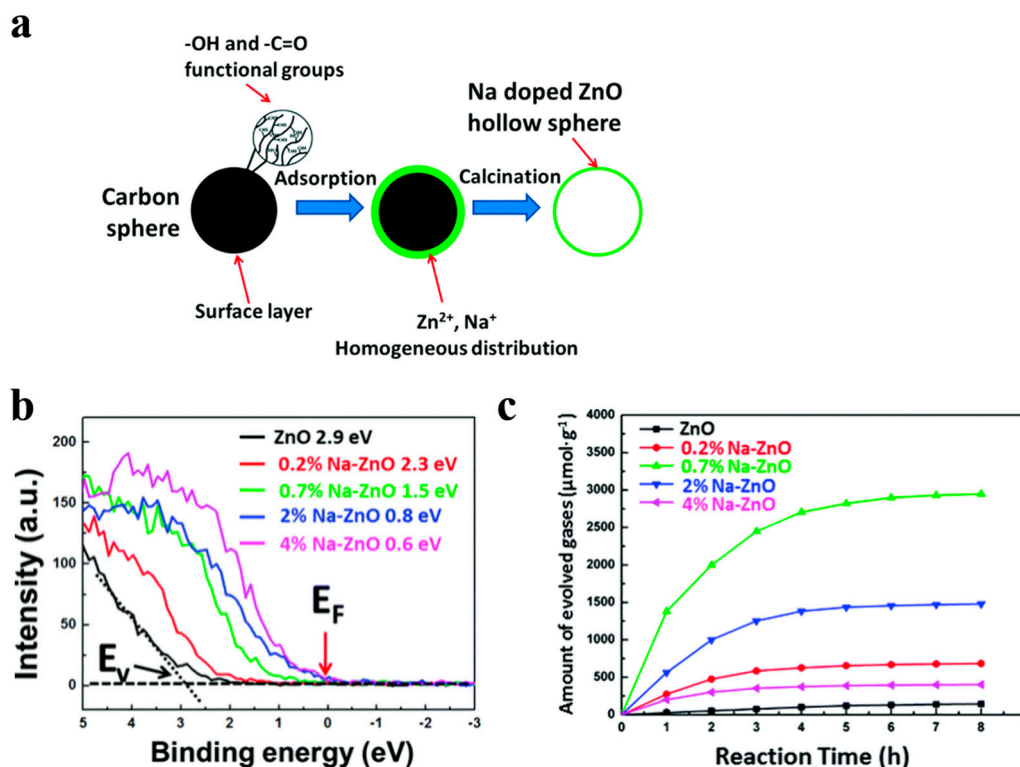


Figure 4. (a) Schematic route for preparing Na-ZnO hollow nanostructures, (b) valence band measure of Na-ZnO with various Na doping concentrations, (c) corresponding H₂ generation for Na-ZnO/Pt hollow spheres with 0, 0.2, 0.7, 2, and 4 at % Na. Reproduced with permission from [53]. Copyright Royal Society of Chemistry, 2016.

Rare earth metals also play a vital role in metal doped semiconductor-based photocatalysts. According to Chao et al. [54], Nd³⁺ led to defects in the lattice which were acted as electron traps, and also could band with non-bridging O²⁻ around the network structure. Nd³⁺ doping could make a red shift of absorption spectrum for TiO₂. In another study [55], they used cerium instead of neodymium to dope into titania hollow spheres. Ce⁴⁺ ions could trap the excited electrons and then electrons would be transferred to adsorbed oxygen on the surface like the reaction



With the increase of Ce⁴⁺ doping content, the space charge layer would be thinner, which efficiently separates electron-hole pairs.

Among all the non-metals used as dopant materials by using carbon spheres templating, carbon doping is relatively common. Carbon spheres are used as hard template and also provide a source of carbon doping. Shi et al. reported C-doped titania nanostructures and its photocatalytic application in 2012 [56]. They presented the preparation of carbon doped TiO₂ nanostructures with a hierarchical macroporous channel structure (Figure 5a), which showed high photocatalytic degradation performance. In another work [57], they deduced the formation mechanism of hollow 3D network structure (Figure 5b), because the surface of carbon spheres was hydrophilic. Carbon doping narrowed the band gap of titania, and hollow 3D structure offered a pathway for guest molecules and enhanced the light harvesting. Recently, Shi's group [58] realized C₃N₄ decorated carbon-doped TiO₂ by in situ growth (Figure 5c). C doping influenced the energy band structure of TiO₂ to enhance photocatalytic activity for application in hydrogen generation under simulated sunlight. Except carbon doping, there are

a few works on non-metal doped semiconductor-based photocatalysis in hollow nanostructure, such as Br-doped TiO₂ [59].

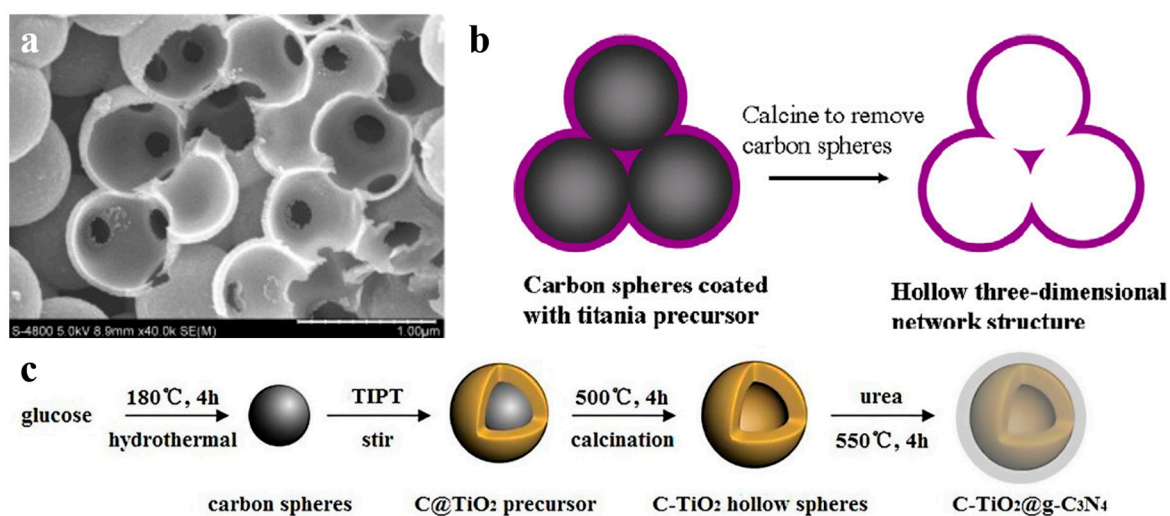


Figure 5. (a) SEM (scan electron microscope) image of broken TiO₂ nanospheres with a macroporous channel structure by crushing THS. Reproduced with permission from [56]. Copyright WILEY, 2012. (b) Formation mechanism of the porous channels in the hollow 3D network structure. Reproduced with permission from [57]. Copyright Elsevier, 2012. (c) Schematic route for preparing C-TiO₂@g-C₃N₄. Reproduced with permission from [58]. Copyright Elsevier, 2017.

In addition to being visible-light absorption centers, dopant also could reduce recombination losses in photocatalyst by trapping photo-generated carriers. Reciprocally, it enhanced the carriers separation to obtain the superior photocatalytic performance. The non-selectively adsorption of carbon sphere template provides a good condition for various doping. For instance, Li et al. [60] described that Fe-doped LaTiO₂N nanostructures exhibited high efficiency, because doping can match the level of conduction band between cocatalysts and LaTiO₂N hollow nanostructures by creating empty mid-gap states in Fe doped LaTiO₂N. As shown in Figure 6a, Fe dopants created a defect level lower than the level of conduction band both of LaTiO₂N and CoO_x, so that the photo-generated electrons could be gathered to CoO_x nanoparticles. As a result, the sample with 1.5% Fe doping exhibited quantum efficiency as high as 55% for O₂ evolution which was fairly higher than other LaTiO₂N system (Figure 6b). Besides, dopant also can reduce the defect sites, where are electron–hole recombination’s sites. Gao et al. [61] found that Mg dopants could not create new trapping states in TiO₂ because it does not have d orbit, but the intrinsic defect states like oxygen vacancy (*V_o*) could be suppressed by Mg doping (Figure 7a). Moreover, the 2p orbit of Mg dopant apart from the level of conduction and valence band of TiO₂ could change the level of defect states by hybridizing the oxygen vacancy in titania (Figure 7b). Besides, as a narrow band-gap semiconductor, Ta₃N₅ also has numerous photo-generated carrier recombination centers, which seriously impairs its photocatalytic activity. Recently, Xiao et al. [62] prepared Mg-doped Ta₃N₅ hollow spheres using carbon spheres templating. Mg ions doped into Ta₃N₅ could not only increase the charge mobility but also tune the electronic structure to promote the charge transportation. From the result of Mott–Schottky measurement (Figure 7c), Mg-Ta₃N₅ had a higher electron density. Theoretically, Mg ions acted as an electron acceptor in Ta₃N₅ photocatalysts. Mg doping was relatively efficient strategy, its photocatalytic hydrogen production is about 7.6-times that of pristine Ta₃N₅ (Figure 7d).

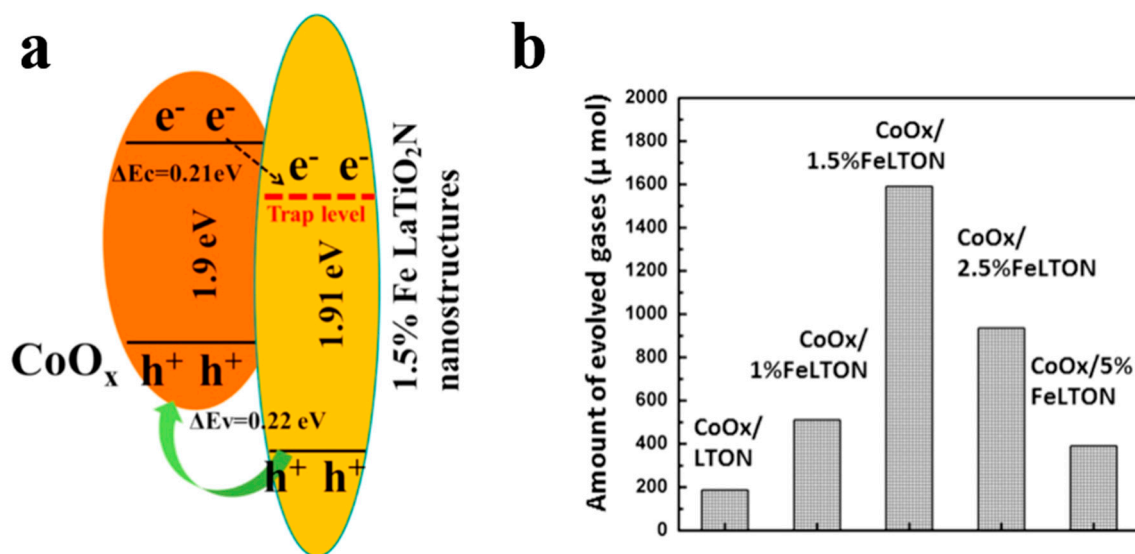


Figure 6. (a) Band energy diagram of $\text{CoO}_x/\text{LaTiO}_2\text{N}$ with 1.5% Fe, and (b) oxygen generation rates for samples with various Fe doping concentration under visible light illumination. Reproduced with permission from [60]. Copyright Elsevier, 2016.

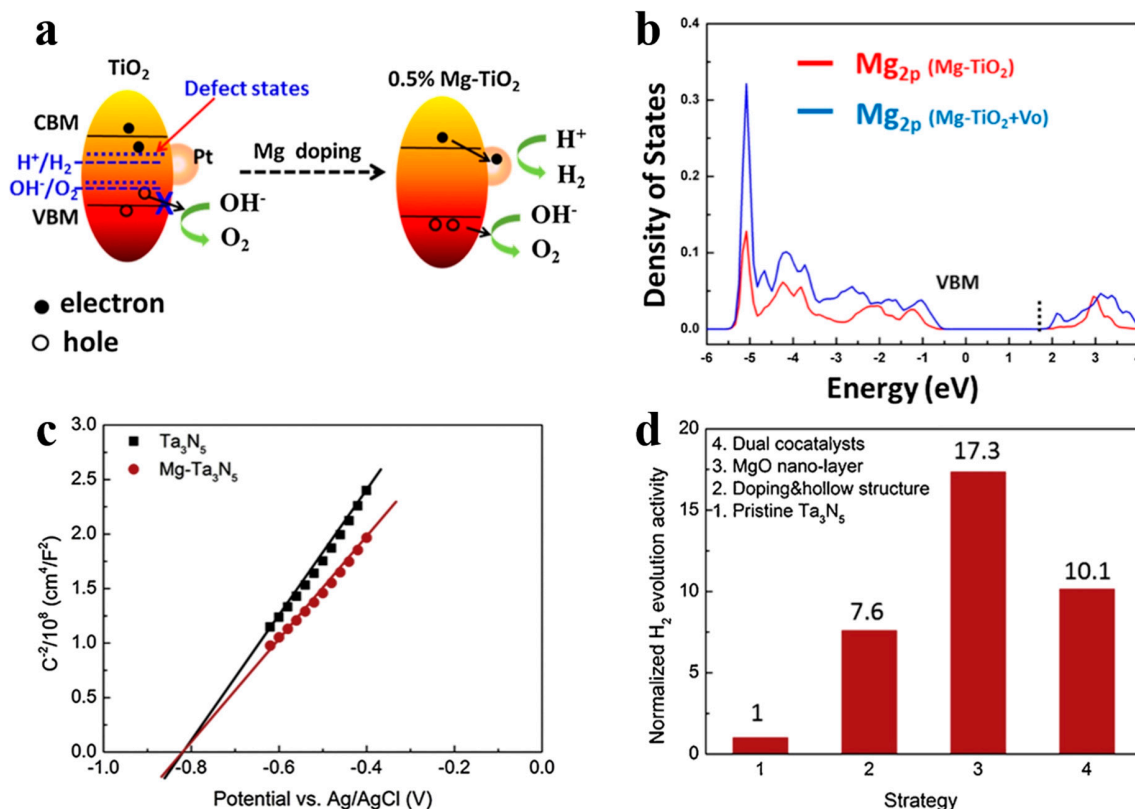


Figure 7. (a) Schematic illustration of the band structure of anatase TiO_2 with and without Mg doping for water splitting. (b) The density of states of Mg 2p in different samples. Reproduced with permission from [61]. Copyright Elsevier, 2017. (c) Mott–Schottky plot of Ta_3N_5 with and without Mg dopant in dark, and (d) normalization of the contribution of individual strategy to the photocatalytic activity. Reproduced with permission from [62]. Copyright Elsevier, 2019.

Researchers have successfully achieved the doping of different elements in various materials by using carbon sphere template method. According to the results, the distribution of doping elements is uniform and there is no phase separation. For some doping systems that cannot be achieved by

other preparation methods, we can try to achieve it by the non-selective adsorption of carbon sphere templates. This also provides ideas for other systems such as single atomic catalysis. Different kinds of salts can be used to make the expected elements adsorb and anchor on the surface of the template, and metal particles with good dispersion may be obtained through subsequent treatment.

3.2. Solid Solution

The bandgap engineering of a semiconductor is very important for its application in various aspects. It not only determines the optical absorption edge and emission wavelength of the material, but also closely related to the electrical conductivity [63]. However, it is difficult to find some semiconductors in nature whose bandgaps fit the requirements of various applications precisely, and that makes bandgap engineering an indispensable study. In order to tailor the bandgap and optoelectronic property of semiconductors, scientists have come up with two main solutions, including doping and forming solid solutions (Figure 8) [64]. The doping method has been described above. Forming solid solutions is to synthesize two or more different semiconductors (with similar crystal or electronic structure) into one material, and the bandgap-controllable solid solutions can be obtained by fine-tuning the content of different components. When applied to photocatalysis, the band gap is expected to be quite narrow while satisfying the potential of the catalytic reaction. Similar to the strategy of doping in previous section, carbon sphere template's uniform and non-selective adsorption of metal ions also enables the synthesis of solid solution hollow nanostructure. By precisely controlling the precursor concentration, a broad solid solubility can be achieved.

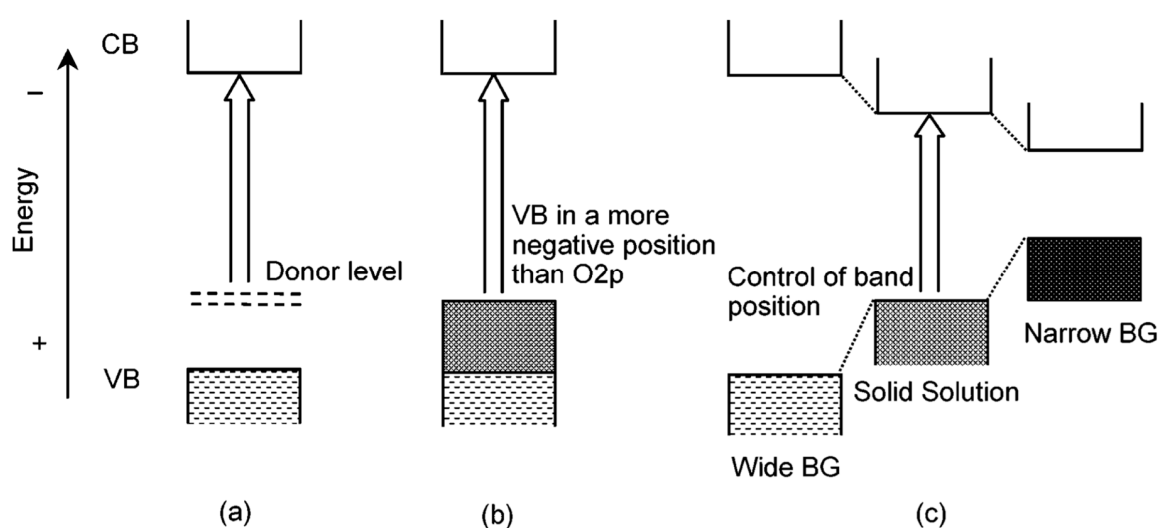


Figure 8. Band engineering through doping and forming solid-solution. (a,b) Formation of a new VBM by doping a foreign element to create a donor level, and (c) forming solid solution to obtain a controllable bandgap. Reproduced with permission from [64]. Copyright American Chemical Society, 2004.

$(\text{Ga}_{1-x}\text{Zn}_x)(\text{N}_{1-x}\text{O}_x)$ is formed by GaN and ZnO. Unlike a solid solution synthesized by a wide and a narrow band semiconductor, GaN and ZnO both have wide bandgaps, while their solid solution has a narrow bandgap about 2.58 eV when the content of ZnO is 13.3% [65]. It is calculated that the VBM (valence band maximum) is composed of Zn 3d orbitals and N 2p orbitals, and the repulsion of electrons of Zn 3d and N 2p result in the narrowing of the band gap [66], which makes the material more suitable for photocatalysis than sole GaN and ZnO. The water-splitting quantum yield of the bulk $(\text{Ga}_{1-x}\text{Zn}_x)(\text{N}_{1-x}\text{O}_x)$ is limited by carrier migration, trapping and recombination. Maeda et al. [67] enhanced the quantum efficiency to 5.9% at 420–440 nm by surface modification, optimizing annealing temperature and composition x of bulk $(\text{Ga}_{1-x}\text{Zn}_x)(\text{N}_{1-x}\text{O}_x)$. Many scientists have improved the overall conversion efficiency of the system by preparing nanomorphological materials.

Reinert et al. [68] obtained nanorods arrays with diameter of about 100 nm. Their $\text{Ga}_2\text{O}_3(\text{ZnO})_{16}$ precursor was heat-treated and cooled under NH_3 flow. By reducing the synthesis temperature to 850°C , the volatilization of Zn was also greatly reduced, thus increasing the x value from <0.42 to 0.55 [65], and reducing the band gap to 2.53 eV . Li et al. [69] synthesized $(\text{Ga}_{1-x}\text{Zn}_x)(\text{N}_{1-x}\text{O}_x)$ nano-hollow spheres by ion adsorption and templating. They used carbon spheres as templates, DMF as solvent, supplemented with the subsequent nitridation, and obtained various composition of $(\text{Ga}_{1-x}\text{Zn}_x)(\text{N}_{1-x}\text{O}_x)$ by adjusting the ratio of the Zn source to the Ga source, tuning the composition of ZnO to the full range from 0.18 to 0.95 . The magnified TEM image (Figure 9a) shows the nano-hollow-spheres, whose diameter are approximately $100\text{--}120\text{ nm}$ and the shell of the sphere is about 7 nm thick. Figure 9c indicates that using this new synthetic method, the narrowing of the bandgap is related to the mutual approachment of both VBM and CBM (conduction band minimum). The nitridation temperature was only 600°C attributing to the the nanoscale hollow structures, much lower than that of bulk form which is approximately 900°C [70], thus it reduces the volatilization of Zn. This nanoscale structure also decreases the carrier diffusion distances and increases the number of reaction sites, enhancing the quantum efficiency to 17.3% (400 nm), which was about 3 times higher than bulk $(\text{Ga}_{0.82}\text{Zn}_{0.18})(\text{N}_{0.82}\text{O}_{0.18})$ [67].

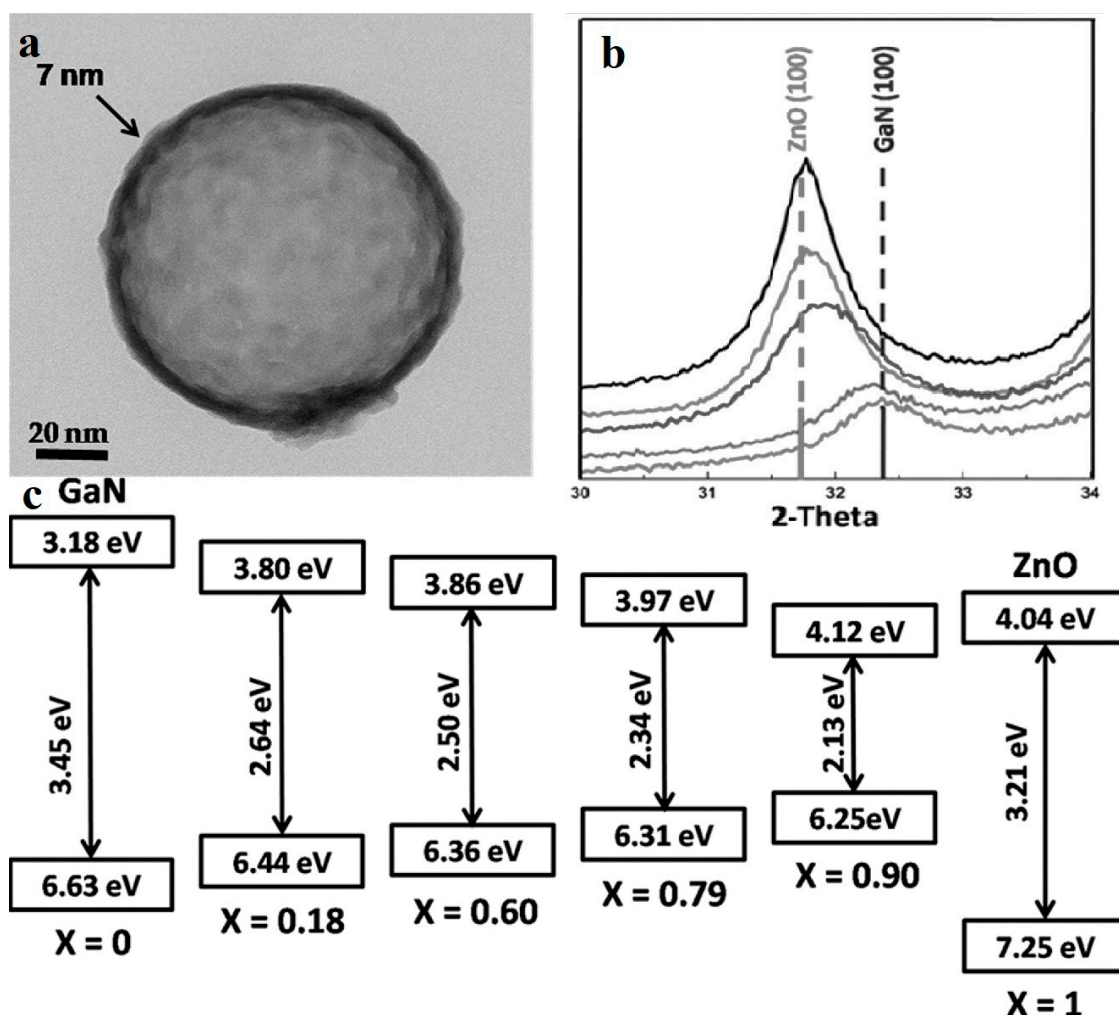


Figure 9. (a) TEM image shows an extremely thin shell (about 7 nm) of $(\text{Ga}_{0.82}\text{Zn}_{0.18})(\text{N}_{0.82}\text{O}_{0.18})$ hollow spheres. (b) The (100) peak shift between GaN (100) and ZnO (100) with different x . (c) The band structure of the $(\text{Ga}_{1-x}\text{Zn}_x)(\text{N}_{1-x}\text{O}_x)$ nanostructures with different x . Reproduced with permission from [69]. Copyright WILEY, 2015.

A similar situation exists in some other solid solution systems. $Zn_xCd_{1-x}S$ is a solid solution composed of CdS and ZnS, which not only has tunable band gap, but also has better photocorrosion resistance and higher photocatalytic activity than pure CdS [71,72]. Gholipour et al. [73] synthesized $Zn_xCd_{1-x}S$ hollow spheres by a solvothermal method, using glycerin to obtain carbon microspheres [74], which contains large amount of OH radicals that can adsorb Zn^{2+} and Cd^{2+} . After centrifuged, calcinated and calcinated in H_2S/Ar flow, the $Zn_xCd_{1-x}S$ hollow spheres can finally be obtained. The value of x can be tuned by adjusting the ratio of zinc source to cadmium source.

The nanostructure of $Zn_xCd_{1-x}S$ is hollow sphere with an average diameter of 500 nm (Figure 10a,b). With the increase of Cd content, the absorption edge moves towards longer wavelength (Figure 10c), indicating the decrease of bandgap. At the same time, the XRD (X-ray diffraction) peak of the samples gradually shifted to lower angle (Figure 10d), accounting for the transformation from hexagonal ZnS to hexagonal wurtzite CdS. The hydrogen evolution they received is as high as $12 \text{ mmol h}^{-1} \text{ g}^{-1}$ under solar irradiation using MoS_2 as cocatalyst. The calculated quantum efficiencies (QE) reached to 46.6% at 400 nm, which was among the highest QE in this system.

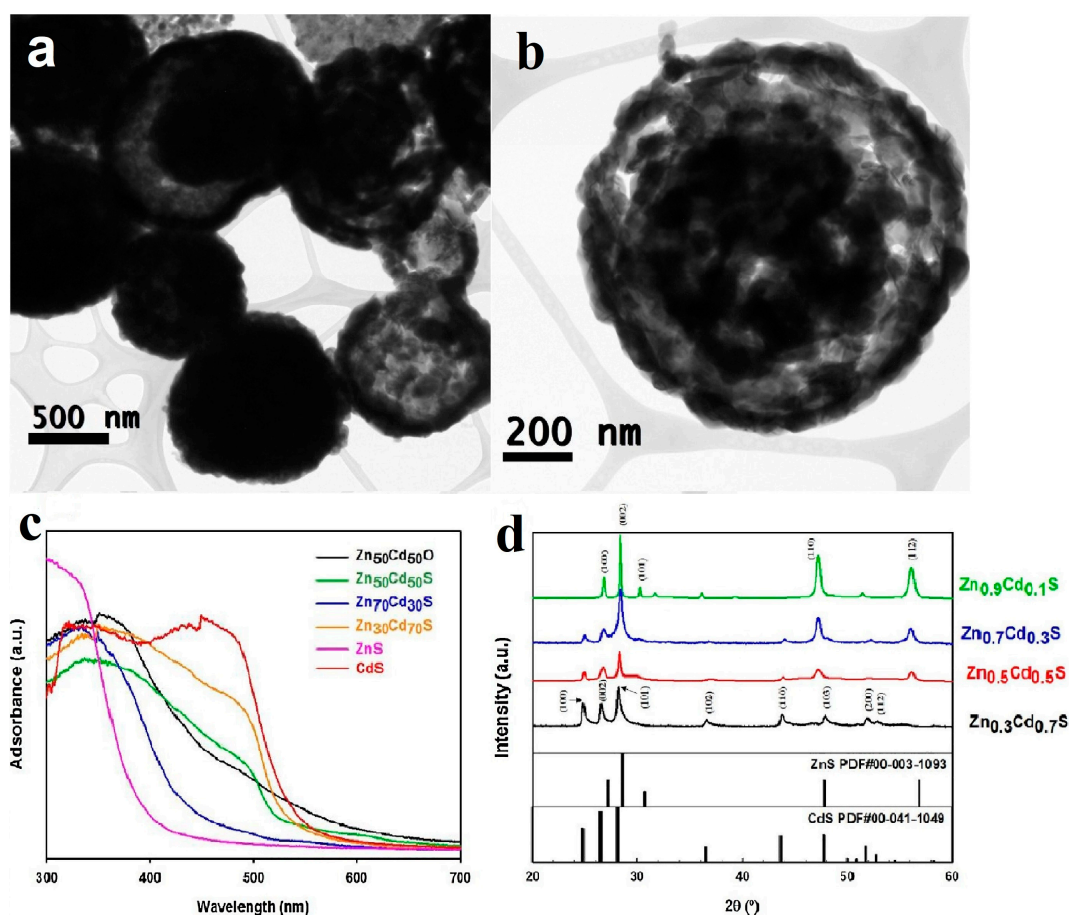


Figure 10. (a,b) TEM images of $Zn_xCd_{1-x}S$ hollow sphere. (c) UV-vis spectra of: $Zn_{0.5}Cd_{0.5}O$, $Zn_{0.5}Cd_{0.5}S$, $Zn_{0.7}Cd_{0.3}S$, $Zn_{0.3}Cd_{0.7}S$, ZnS, and CdS (d) XRD patterns of solid solutions of $Zn_xCd_{1-x}S$ after H_2S treatment. Reproduced with permission from [73]. Copyright Elsevier, 2018.

So far, there are few solid solution systems realized by carbon sphere template method. By adjusting the precursor and subsequent treatment, this method may be able to achieve more solid solution hollow nanostructures.

3.3. Heterostructure

It is hardly for individual semiconductor materials to satisfy fundamental requirements of highly efficient photocatalysts, such as suitable bandgap for effective sun light absorption, proper charge separation, high carrier mobility and fast kinetics for surface reaction [75,76]. Introducing heterojunction comes to be a potential strategy to meet these critical requirements simultaneously by combining the advantages of two or more semiconductors. A conventional heterojunction is established by coupling two semiconductors having suitable structures of energy band directly. Heterostructured hollow photocatalysts have received growing research attention by cause of their unusual advantages such as ultrahigh sunlight absorption, extremely large surface area and short carrier transfer distance in recent year [76,77]. So far, heterostructured hollow photocatalysts have demonstrated great application potential in varied photocatalytic fields [49,78]. Due to the good adsorption capacity of carbon sphere template, we are able to obtain hollow nano heterostructures by multiple adsorption and different annealing conditions.

Semiconductor-based photocatalysts applied in water splitting are identified as the most economic and environmentally friendly material systems for hydrogen production [79]. In recent years, a great deal of previous research spotlighted on water splitting based on advanced heterostructured hollow photocatalysts.

For instance, Song et al. [80] demonstrated the superior photocatalytic H₂ evolution activity of ZnFe₂O₄/ZnO hollow nanoheterostructures by a facile hard-templating approach. The nanoheterostructures of ZnFe₂O₄/ZnO, which are about 15 nm in size, are homogeneously distributed in the hollow sphere shell. The champion sample without the help of co-catalysts exhibits an outstanding H₂ evolution rate of 2.15 mmol h⁻¹ g⁻¹ when irradiated by visible light. The corresponding quantum efficiency reaching 1.61%, which is 7.6 times higher than that of bare hollow ZnFe₂O₄ photocatalysts. ZnO forms a type-II heterojunction with ZnFe₂O₄ in the sphere shell (Figure 11) which confirmed by the combination investigation of XPS (X-ray photoelectron spectroscopy) technic as well as UV-vis diffuse reflectance spectroscopy. The photogenerated electrons and holes will be separated into the conduction band of ZnO and valence band of ZnFe₂O₄ by the built-in electric field, respectively, thereby minimizing the recombination and boosting the photocatalytic H₂ generation performance of samples. Meanwhile, Li et al. [81] have reported a high-crystallinity g-C₃N₄/TiO₂ hollowsphere nanoheterojunction photocatalyst with large surface area through a carbon sphere templating method. By carefully tuning the ratio of precursors, the optimum g-C₃N₄/TiO₂ photocatalyst obtain a 5.5-fold enhancement in visible-light-driven hydrogen generation rate, reaching almost 470 μmol g⁻¹ h⁻¹. The improvement in photocatalytic performance primarily owes to the establishment of heterojunctions which accelerating carrier's separation efficiently confirmed by PL spectrum and electrochemical independence spectroscopy. While conventional heterojunctions are generally in form of crystalline/crystalline contact, Lou et al. [82] have investigated a novel type of crystalline/amorphous heterostructure. A crystalline Cu₂O/amorphous Ta₂O₅ heterostructure fabricated by a two-step ion absorption approach based on carbon spheres template. Such heterostructures were found to possess the capacity for splitting water into H₂ and O₂ driven by visible light without using sacrificial agent. Theoretical calculation shows the existence of hole trap states in the crystalline/crystalline interface cause by lattice and electron mismatch, which does not exist at the crystal/amorphous interface (Figure 12). Moreover, the type-II heterojunction of crystalline Cu₂O/amorphous Ta₂O₅ greatly promotes the separation of photo-induced charges to perform effective overall water splitting.

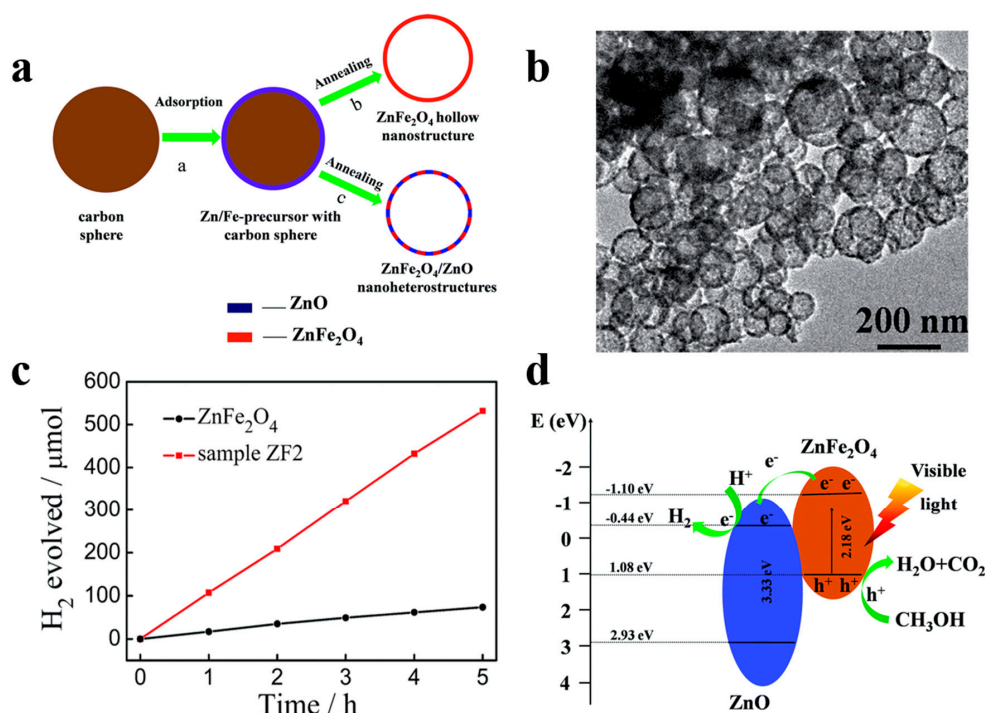


Figure 11. (a) Schematic diagram of preparation process of ZnFe₂O₄ nanostructures and ZnFe₂O₄/ZnO nanoheterostructures. (b) TEM images of ZnFe₂O₄/ZnO spheres. (c) H₂ production over time by 50 mg photocatalysts of bare ZnFe₂O₄ and ZnFe₂O₄/ZnO (ZF2) sample driven by visible light (>420 nm). (d) Schematic illustration of ZnFe₂O₄/ZnO heterojunction energy band position and predicted reaction mechanism under irradiation. Reproduced with permission from [80]. Copyright Royal Society of Chemistry, 2015.

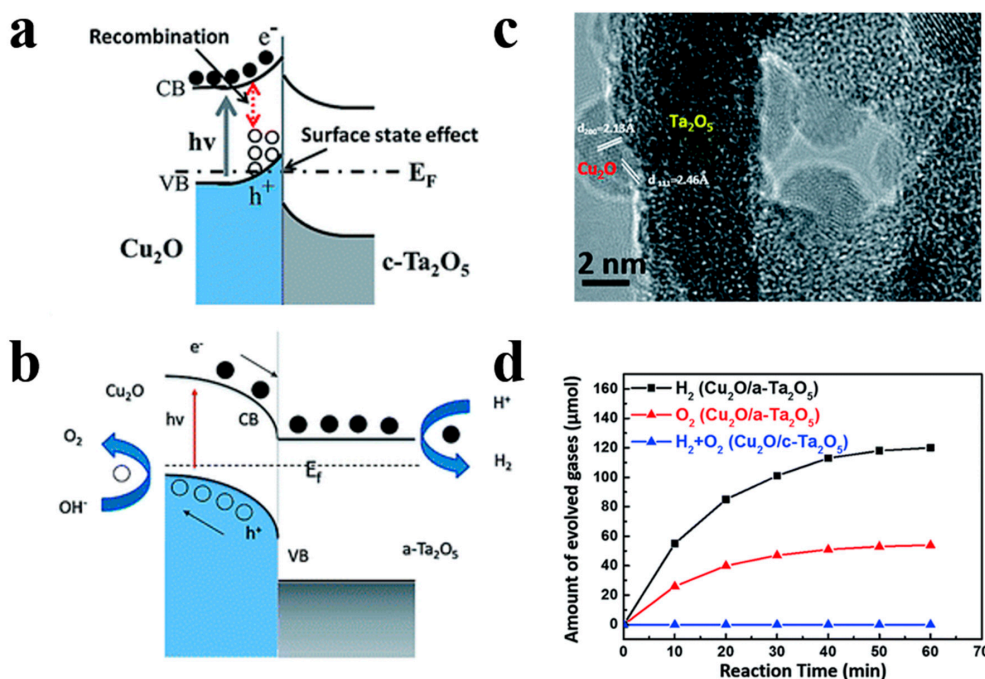


Figure 12. (a) Band bending diagram of Cu₂O/crystalline Ta₂O₅. (b) Band bending diagram of Cu₂O/amorphous Ta₂O₅ nanoheterojunctions. (c) HRTEM image of Cu₂O/amorphous Ta₂O₅ heterostructures. (d) Amount of evolved gases under full light for different samples. Reproduced with permission from [82]. Copyright Royal Society of Chemistry, 2017.

In addition, other research groups also have reported hollow heterojunction photocatalysts with high performance. Waqas et al. [83] prepared hollow sphere $\text{TiO}_2/\text{Fe}_2\text{TiO}_5$ heterojunction photocatalyst through a simple two-step templating method for high efficient solar water oxidation. The oxygen evolution reaction rate of the champion sample with 35% Fe reached $375 \mu\text{mol h}^{-1} \text{g}^{-1}$ benefited from the desirable energy band alignment of $\text{TiO}_2/\text{Fe}_2\text{TiO}_5$ heterojunction, which improved carrier separation in these photocatalysts. In another work, heterostructured $\text{ZnFe}_2\text{O}_4/\text{ZnSe}$ hollow sphere photocatalysts which were synthesized through two-step carbon templating approach used in visible-light-driven water splitting [84]. Heterostructured ZnSe photocatalysts with suitable shell thickness generated a large amount of H_2 of 16.9 mmol g^{-1} in 6 h, owing to the effective charge separation and accelerated carrier transfer.

Hollow nanoheterostructured photocatalysts possess extremely large surface area, high catalytic activity and carrier separation efficiency, thus being suitable for application of pollutant degradation [49,75,77,85].

In 2014, Li et al. [86] have pioneered a simple and universal method for fabricating a hybrid hollow nanoheterostructured photocatalyst with ultrathin shell. Taking the $\text{TiO}_2/\text{SnO}_2$ hollow sphere photocatalyst as a typical example, they mixed 0.5 g of carbon spheres and a proper amount of $\text{C}_{16}\text{H}_{36}\text{O}_4\text{Ti}$ and $\text{SnCl}_2 \cdot 2\text{H}_2\text{O}$ together and stirred for 24 h, followed by rinsing and drying in an oven at 80°C for 6 h. The $\text{TiO}_2/\text{SnO}_2$ hybrid nanostructured hollow spheres finally obtained by calcination have 3–10 nm small grain size and ultrahigh surface area of $300 \text{ m}^2 \text{ g}^{-1}$. Compared to single TiO_2 and SnO_2 hollow nanostructured photocatalysts, the $\text{TiO}_2/\text{SnO}_2$ hybrid hollow nanostructured photocatalyst shows a superior RhB dye photodegradation activity, which is profited from the built-in electric field induced by $\text{TiO}_2/\text{SnO}_2$ heterojunction as well as the short carrier diffusion length in $\text{TiO}_2/\text{SnO}_2$ nanocrystal (Figure 13). Adopting a similar strategy, Lou et al. [87] have also successfully prepared a hollow $\text{Fe}_2\text{TiO}_5/\text{TiO}_2$ nanoheterostructure to enhance the photocatalytic performance of TiO_2 -based photocatalysts driven by visible light. The favorable energy band alignment of $\text{Fe}_2\text{TiO}_5/\text{TiO}_2$ heterojunction suppressed the carrier recombination significantly. As a result, the optimum nanoheterostructured photocatalyst exhibited a 3-times higher visible-light photocatalytic-degradation activity towards RhB compared to that of commercial P25 photocatalyst.

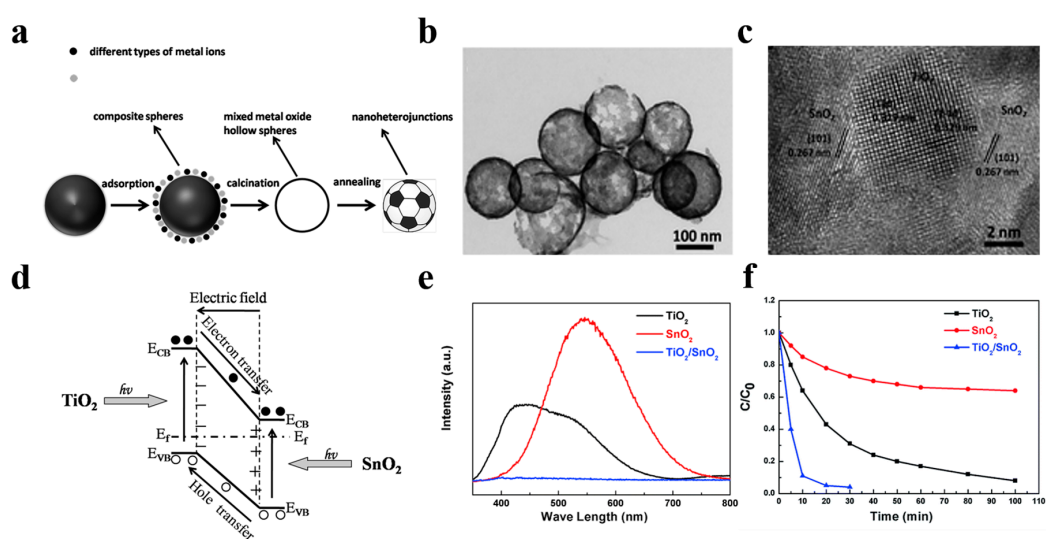


Figure 13. (a) Schematic illustration of the formation path of nanoheterostructured photocatalysts. (b) TEM image of the $\text{TiO}_2/\text{SnO}_2$ hybrid nanostructure. (c) HRTEM images of the $\text{TiO}_2/\text{SnO}_2$ nanoheterojunctions. (d) Schematic illustration of band structure of $\text{TiO}_2/\text{SnO}_2$ heterojunction. (e) The PL spectra of three different hollow spheres, red line for SnO_2 , black line for TiO_2 , and blue line for $\text{TiO}_2/\text{SnO}_2$. (f) The photocatalytic activity measurement of different structures towards RhB under full light irradiation. Reproduced with permission from [86]. Copyright Royal Society of Chemistry, 2014.

Diversification of structural morphology makes hollow sphere photocatalysts more attractive. Ang et al. [85] have reported multi-dimensional hierarchical hollow heterojunctioned CuO/TiO₂ spheres with TiO₂ thorns grown on the surface of CuO hollow spheres by a carbon spheres assisted template method (Figure 14a,b). The hierarchical TiO₂ thorns acted as water channels generating a mass of reactive oxygen species for pollutant degradation. The multi-dimensional CuO/TiO₂ spheres show an excellent photodegradation activity in comparison to P25 thanks to the effective carrier separation and migration origin from the establishment of CuO/TiO₂ heterojunction. Liu et al. [88] have successfully used a microwave-assistant carbon sphere templating method to synthesize hollow nest-like γ -Fe₂O₃/ZnO photocatalysts, which ZnO nanosheets were loaded on the shell of γ -Fe₂O₃ hollow spheres (Figure 14c,d). The large surface area and effective restraint of carrier recombination of γ -Fe₂O₃/ZnO result in an enhanced photocatalytic activity compared with bare ZnO photocatalysts.

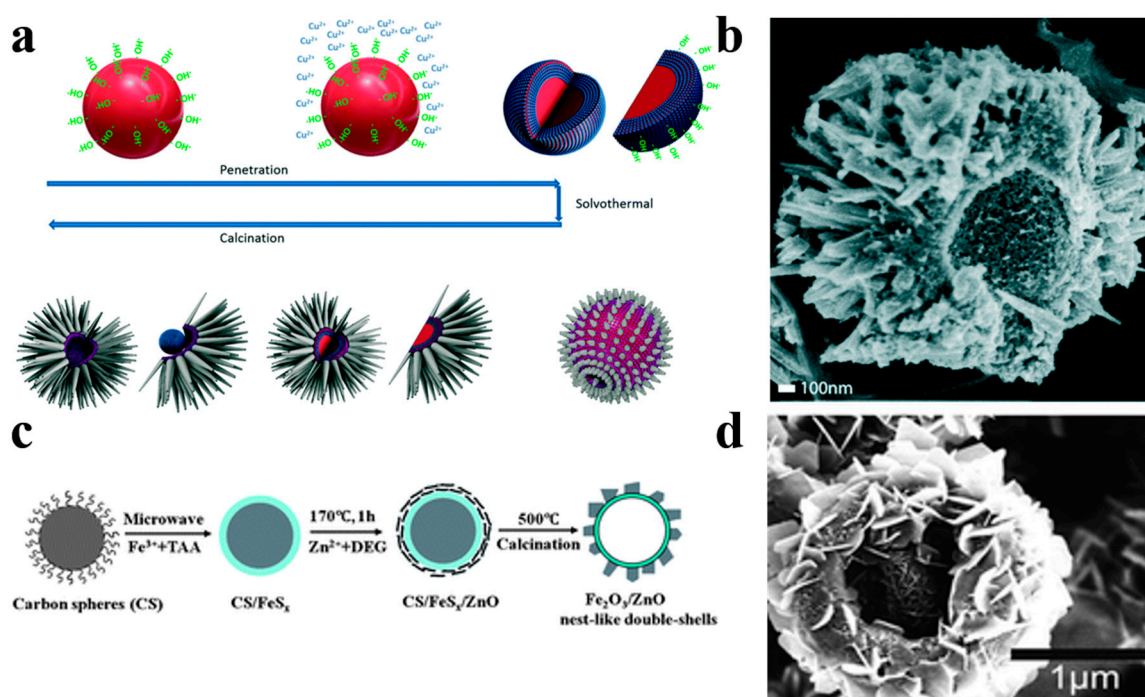


Figure 14. (a) Schematic diagram of the fabrication process of hollow hierarchical CuO/TiO₂ structure. (b) SEM image of the CuO/TiO₂ spheres. Reproduced with permission from [85]. Copyright 2017, RSC. (c) Schematic diagram of the preparation process of nest-like γ -Fe₂O₃/ZnO hollow nanostructures. (d) SEM images of γ -Fe₂O₃/ZnO nest-like hollow nanostructures. Reproduced with permission from [88]. Copyright Royal Society of Chemistry, 2012.

Other type-II hollow heterostructured photocatalysts derived from carbon sphere template such as CeO₂/TiO₂ [89], WO₃/TiO₂ [90], ZnO/CuO [91], ZnO/SnO₂ [92], and ZnO/ZnS [93] also showed enhanced photocatalytic pollutant degradation performance by the promotion of heterojunction.

Nanoheterostructure is one of the most facilely realized structures by carbon sphere template method. One-step adsorption by the carbon sphere template can realize heterostructure on the same spherical shell, and multi-step adsorption can realize hollow spherical nanostructures with core-shell distribution or multilayer structure. Notably, as powder photocatalysts, recycling is a very important issue. Generally, we build a heterostructure with magnetic materials to achieve magnetic recycling. However, magnetic materials generally have low photocatalytic activity and light blocking, which will reduce the efficiency of light utilization. By carbon sphere template method, the magnetic materials may be confined in the hollow nanospheres of photocatalyst by the method of multi-step adsorption, so as to realize the light utilization efficiency and recyclability.

3.4. Surface Modification

For photocatalysis, the more electron–hole pairs are photogenerated and come into play, the higher the efficiency will be. However, the recombination is proven to harmfully impede the process of water-splitting or degradation resulting in a low efficiency [27,37,82]. Hollow structures can shorten the transport distance of carries from bulk to their proper catalytic sites on the surface, which suppress bulk recombination tremendously [37,77]. However, a majority of surface defects remain there and behave as another kind of recombination centers [94]. Meanwhile the extra electronic and optical states may have an influence on electronic structure or band structure [95]. Surface modification is the most effective measure to suppress surface recombination and increase active sites. Carbon sphere templates can absorb precious metals uniformly in solution, and also can be used as good skeleton support in subsequent treatment. The carbon sphere template derived ultra-thin hollow nanostructure also provides favorable conditions for the subsequent surface modification. Furthermore, combining surface modification and hollow structure will endow photocatalysts with both higher activity and better stability.

The introduction of disorder at the surface of photocatalysts is a common method of surface modification. It has been revealed that lattice disorder in semiconductors could yield band tail states. It would dominate the optical excitation and relaxation, and provide intended trapping sites for photo-generated carriers to avoid rapid recombination [96,97]. Chen et al. [96] prepared TiO₂ nanocrystals with disordered surface layers via hydrogenation and found that it could help harvest infrared optical photons and contribute to organic molecules photo-oxidation and H₂ evolution. Li et al. [95] reported a surface-reconstructed hollow LaTiO₂N nanostructure with significantly improved photocatalytic activity (Figure 15). The ultrathin hollow LaTiO₂N spheres were firstly synthesized by utilizing carbon spheres as hard templates. Then H₂ treatment was carried not only to load the cocatalyst Pt but also to modify the surface of LaTiO₂N spheres. Pt/H-LTON achieved a remarkably improved H₂ evolution rate (up to 192 μmol h⁻¹, compared to 91 μmol h⁻¹ of Pt/LTON) and stability. Interestingly, the contrast sample with extra N₂ annealing, which maintained the presence of Ti³⁺ ions but removed the disordered surface even exhibited worse photocatalytic performance than Pt/LTON. It indicated that the excellent photocatalytic capacity for water splitting was a consequence of the disordered surface rather than the induced Ti³⁺ ions. Introducing H atom can passivate surface defects, thus avoiding a majority of surface recombination of photo-induced carriers [94,95]. Therefore, surface disordering functions as a complementary strategy for improving photocatalytic activity combined with hollow structures.

Oxygen vacancies are also proved to strongly affect photocatalytic activity of metal oxides-based photocatalysts [98]. Black titanium oxide is a typical example, in which electrons transition occurs between levels of valence band of the photocatalyst and the introduced oxygen vacancy states under visible radiation [98,99]. Recently, Song et al. [100] successfully prepared black titanium oxide hollow nanospheres with ultrathin shells for more effective solar-driven water splitting (Figure 16). The high quality TiO₂ possessed a high specific surface area of 168.8 m² g⁻¹ and was obtained by a conventional carbon sphere templating method combined with subsequent Al reduction. This black TiO₂ nanostructure exhibited a much higher photocatalytic H₂ evolution rate (56.7 mmol h⁻¹ g⁻¹), which was well above that of the as-prepared one (22.9 mmol h⁻¹ g⁻¹) when using xenon lamp as irradiation source. It was found that Al reduction introduced masses of oxygen vacancies into TiO₂ which can act as donors and accelerate the separation and transportation of the photogenerated electron–hole pairs.

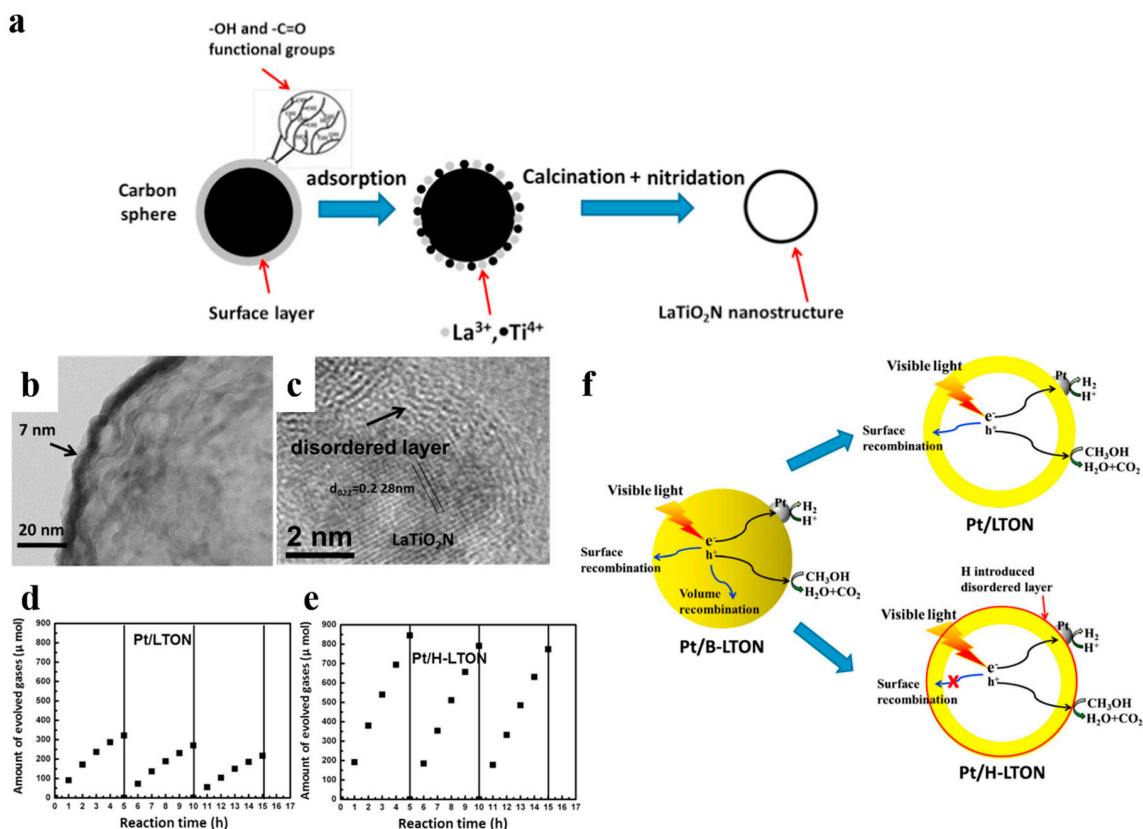


Figure 15. (a) The simple illustration of the synthesizing process of LaTiO_2N nanostructures. (b) TEM image of LaTiO_2N hollow nanostructures. (c) HRTEM image of the H_2 treated LaTiO_2N . (d,e) Hydrogen generation versus time on Pt/LTON and Pt/H-LTON irradiated by visible light ($\lambda \geq 420 \text{ nm}$) respectively. (f) Possible hydrogen generation principles proposed of the Pt/B-LTON, Pt/LTON and Pt/H-LTON respectively. Reproduced with permission from [95]. Copyright Elsevier, 2015.

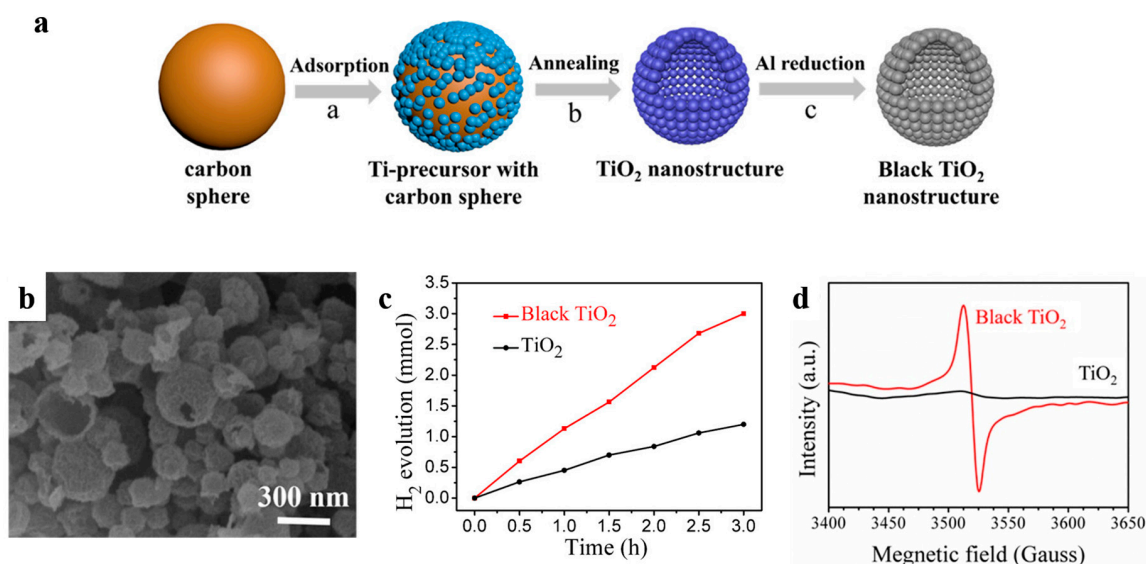


Figure 16. (a) The synthesis process of the as-prepared TiO_2 nanostructures and black ones. (b) SEM image of black TiO_2 . (c) Time course of photocatalytic H_2 evolution of TiO_2 nanostructures. Reaction conditions: 20 mg photocatalysts, 1 wt % Pt loaded, under 300W Xe lamp irradiation. (d) EPR spectra of the as-prepared TiO_2 hollow spheres and black ones. Reproduced with permission from [100]. Copyright American Chemical Society, 2017.

Besides, cocatalysts can help lower energy barriers, enhance photo-generated charge separation and provide reaction sites [101]. Different cocatalysts are designed to facilitate the oxidation or reduction process on the surface respectively [102]. Template method makes it easy to load related cocatalysts to the specified spots of photocatalysts. For example, Li et al. [102] designed Pt@TiO₂@MnO_x hollow spheres to improve the photo-oxidation of water and benzyl alcohol. Xiao et al. [62] reported that the Ta₃N₅ hollow spheres with Pt/CoO_x dual cocatalysts exhibited better photocatalytic ability of water splitting compared with those only with Pt cocatalyst. Hollow TiO₂ modified with spatially isolated Au and CoO dual cocatalysts for CO₂ photoreduction was designed by Zhu et al. (Figure 17) [103]. CoO was formed on the inner surface of carbon spheres by ions absorption, and then Au was decorated on the external surface by Au ions reduction. The optimal formation rate of CH₄ from CO₂ reduction of Au_{2.0}@THS@CoO was nearly 60 times as high as that of TiO₂ hollow nanospheres (THS), while the activity of THS with Au and CoO nanoparticles randomly deposited was not so good. There is convincing evidence that Au and CoO are the suitable co-catalysts for photo-generated electrons and holes respectively so that carriers can be separated effectively on the inner or outer surfaces of the hollow nanostructure. Carbon templating is a convenient way of designing cocatalyst loading.

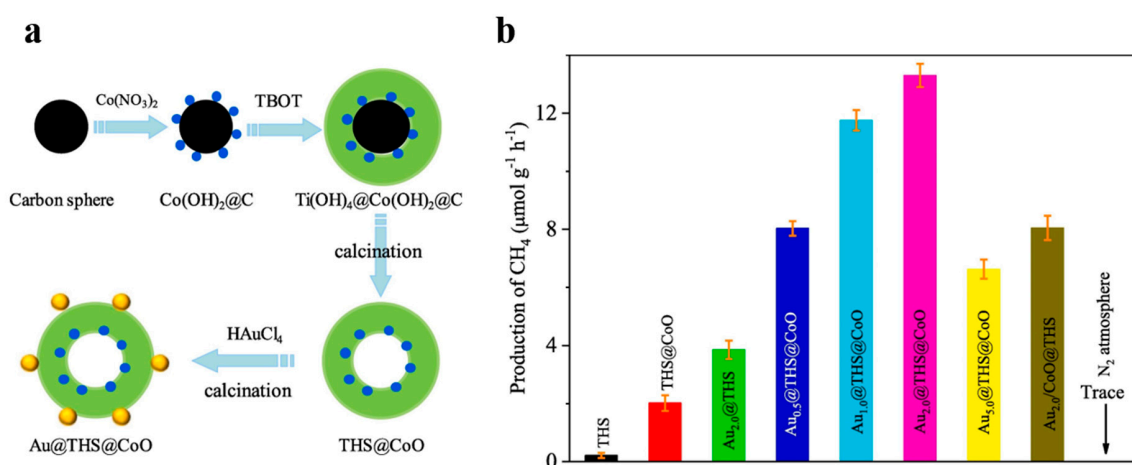


Figure 17. (a) Diagrams of preparation of Au_x@THS@CoO. (b) Production rates of CH₄ for THS, THS@CoO and Au_{2.0}@THS@CoO. Reproduced with permission from [103]. Copyright Elsevier, 2019.

Furthermore, plasmonic metal nanocrystals have been intensively investigated recently on account of its unique optical and electronic properties. Gold (Au) and silver (Ag) can work as cocatalysts as well as light sensitizers in aspect of photocatalysis. Wang et al. [104] synthesized yolk-shell Au@TiO₂ nanostructure by employing carbon spheres as templates (Figure 18). Core-shell Au@C was fabricated through hydrolysis and then it worked as a template to form yolk-shell Au@TiO₂ (Au@TiO₂-YS). The diameter of Au@TiO₂-YS was about 350 nm with the Au core 70–90 nm or so. Evidently, this morphology brought a much larger BET (Brunauer–Emmett–Teller) surface area reaching 128.9 m²/g and a higher content of mesoporous particles than core-shell Au@TiO₂. Owing to plasmonic effects, Au@TiO₂-YS had broader light absorption extended to about 570 nm. It was found to be able to degrade the gaseous toluene more efficiently than the core-shell structure, almost 1.63 times higher. Obviously, the large surface area and abundant mesoporous channels induced by the yolk-shell structure make it easy to absorb more VOCs (Volatile Organic Compounds) and proceed the degradation. In addition, thin shells are also beneficial for photo-generated carriers to separate and migrate and unique cavities increase light reflection and refraction, too, thus enhancing the LSPR (Localized Surface Plasmon Resonance) effect of Au.

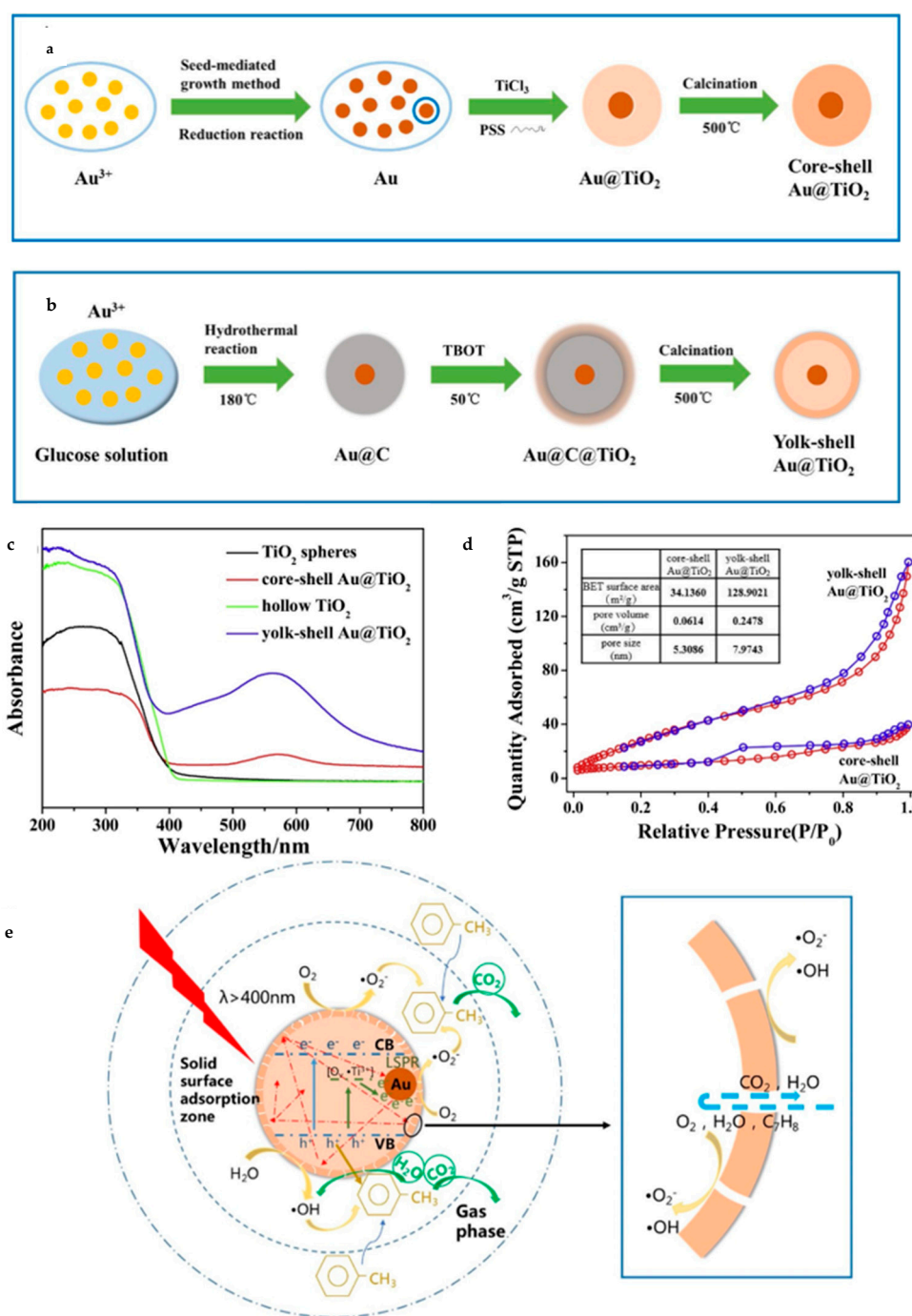
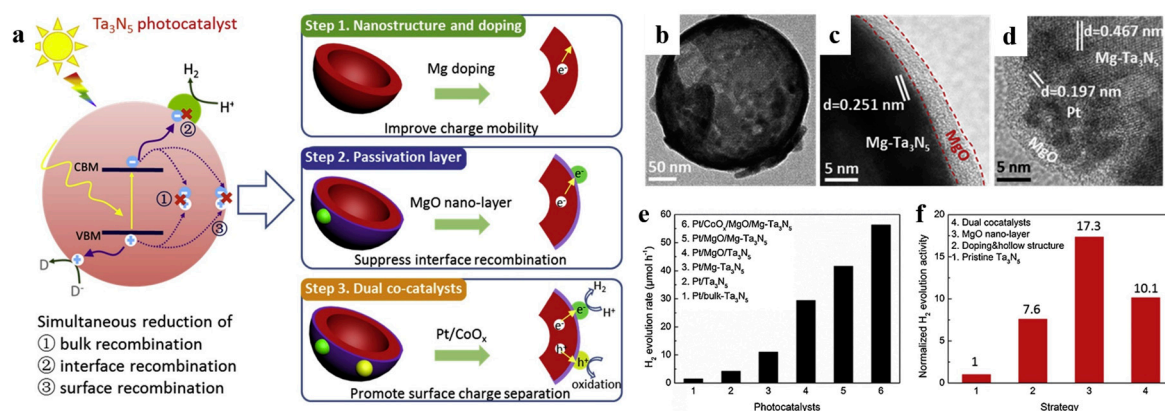


Figure 18. Schematic diagram of synthesis of (a) core-shell, (b) yolk-shell Au@TiO_2 . (c) UV-vis absorbance spectra for different kinds of TiO_2 spheres. (d) The BET curves of yolk-shell and core-shell Au@TiO_2 respectively. (e) The possible photocatalysis principle of Au@TiO_2 -YS. Reproduced with permission from [104]. Copyright Elsevier, 2019.

In addition, passivation layers can also modify the surface of hollow structure. Xiao et al. [62] demonstrated that MgO nano-layer as passivation layer seemed to be an effective strategy for Mg-doped Ta_3N_5 hollow spheres (Figure 19). The Mg-doped Ta_2O_5 precursor fabricated with the aid of carbon spheres templating, and subsequently it was well wrapped in-situ by a thin layer of MgO even less than 5 nm. The particle size of Pt further decreased from 2.04 nm to 1.33 nm along with the deposition of MgO. The increased ratio of hydrogen generation for MgO modification is 17.3 compared to the bulk Ta_3N_5 , mainly due to the efficient charge transfer and passivation of surface defects. It should be noted

that excessive MgO may adversely affect the charge transfer between Ta₃N₅ and cocatalysts instead since MgO is known as an insulator. Therefore, it is necessary to manage the thickness of the passivation layer by controlling the parameters of ion absorption.



Surface modification is not unique to the carbon sphere template method, but the adsorption characteristics of carbon sphere can well realize the delocalization of different co-catalysts. The carbon in the template can also acts as reducing agent. Under different post-treated atmosphere, it can play a role not only as a template. The hollow nanostructures with controllable shell thickness prepared by carbon sphere template method also provide convenience for many subsequent processing. In photocatalysis, the carrier migration distance is a very important factor. The thin shell prepared by carbon sphere template with subsequent surface treatment can greatly improve the efficiency of photocatalyst carrier utilization.

A summary of the recent carbon sphere template derived hollow nanostructure photocatalysts is presented in Table 1.

Table 1. Summary of carbon sphere template derived hollow nanostructure for photocatalysis.

Strategy	Material	Reaction	Efficiency	Reference
Doping	WO ₃ : Fe	RhB degradation	$k_{\text{RhB}} = 0.02 \text{ min}^{-1}$	[52]
	ZnO: Na	H ₂ evolution	1380 $\mu\text{mol g}^{-1} \text{ h}^{-1}$ (AQY = 13.5% @ 350 nm)	[53]
	TiO ₂ : Nd	X-3B degradation	$k_{\text{X-3B}} = 0.0087 \text{ min}^{-1}$	[54]
	TiO ₂ : Ce	X-3B degradation	$k_{\text{X-3B}} = 0.029 \text{ min}^{-1}$	[55]
	TiO ₂ : C	H ₂ evolution	35.6 $\mu\text{mol g}^{-1} \text{ h}^{-1}$	[56–58]
	TiO ₂ : Br	RhB, MO, MB degradation	90% removal in 40 min	[59]
	LaTiO ₂ N: Fe	O ₂ evolution	1.59 mmol h ⁻¹ (AQY = 55% @ 450 nm)	[60]
	TiO ₂ : Mg	Overall water splitting	H ₂ : 850 $\mu\text{mol g}^{-1} \text{ h}^{-1}$ O ₂ : 425 $\mu\text{mol g}^{-1} \text{ h}^{-1}$ (AQY = 19.4% @ 350 nm)	[61]
	Ta ₃ N ₅ : Mg	H ₂ evolution	11 $\mu\text{mol h}^{-1}$	[62]

Table 1. Cont.

Strategy	Material	Reaction	Efficiency	Reference
Solid-solution	$(\text{Ga}_{1-x}\text{Zn}_x)(\text{N}_{1-x}\text{O}_x)$	Overall water splitting	H_2 : $254.2 \mu\text{mol h}^{-1}$ O_2 : $127.1 \mu\text{mol h}^{-1}$ (AQY = 14.3% @ 400 nm)	[69]
	$\text{Zn}_x\text{Cd}_{1-x}\text{S}$	H_2 evolution	$12 \text{ mmol h}^{-1} \text{ g}^{-1}$ (AQY = 46.6% @ 400 nm)	[73]
Heterostructure	$\text{ZnFe}_2\text{O}_4/\text{ZnO}$	H_2 evolution	$2.15 \text{ mmol h}^{-1} \text{ g}^{-1}$ (AQY = 1.61% @ 440 nm)	[80]
	$\text{g-C}_3\text{N}_4/\text{TiO}_2$	H_2 evolution	$470 \mu\text{mol g}^{-1} \text{ h}^{-1}$	[81]
	$\text{Cu}_2\text{O}/\alpha\text{-Ta}_2\text{O}_5$	Overall water splitting	H_2 : $202 \mu\text{mol h}^{-1}$ O_2 : $98 \mu\text{mol h}^{-1}$ (AQY = 3% @ 480 nm)	[82]
	$\text{TiO}_2/\text{Fe}_2\text{TiO}_5$	O_2 evolution	$375 \mu\text{mol g}^{-1} \text{ h}^{-1}$	[83]
	$\text{ZnFe}_2\text{O}_4/\text{ZnSe}$	H_2 evolution	$2.8 \text{ mmol g}^{-1} \text{ h}^{-1}$	[84]
	$\text{TiO}_2/\text{SnO}_2$	RhB degradation	$k_{\text{RhB}} = 0.22 \text{ min}^{-1}$	[86]
	$\text{Fe}_2\text{TiO}_5/\text{TiO}_2$	RhB degradation	$k_{\text{RhB}} = 0.09 \text{ min}^{-1}$	[87]
	CuO/TiO_2	AO7 degradation	$k_{\text{AO7}} = 0.057 \text{ min}^{-1}$	[85]
	$\gamma\text{-Fe}_2\text{O}_3/\text{ZnO}$	RhB, MO, MB degradation	90% RhB, MB removal in 50 min 80% MO removal in 80 min	[88]
	$\text{CeO}_2/\text{TiO}_2$	RhB degradation	75% removal in 180 min	[89]
	WO_3/TiO_2	MB degradation	78% removal in 80 min	[90]
	ZnO/CuO	MB degradation	98% removal in 60 min	[91]
	ZnO/SnO_2	TC degradation	81% removal in 180 min	[92]
	ZnO/ZnS	RhB degradation	99% removal in 40 min	[93]
Surface modification	Surface-reconstructed LaTiO_2N	H_2 evolution	$192 \mu\text{mol h}^{-1}$ (AQY = 3.4% @ 440 nm)	[95]
	Black TiO_2	H_2 evolution	$56.7 \text{ mmol h}^{-1} \text{ g}^{-1}$ (AQY = 90.6% @ 365 nm)	[100]
	$\text{Pt}/\text{TiO}_2/\text{MnO}_x$	Benzyl alcohol oxidation	$31.22 \mu\text{mol}$ in 14 h (AQY = 63.14% @ 254 nm)	[102]
	$\text{Pt}/\text{CoO}_x/\text{MgO}_2/\text{Ta}_3\text{N}_5$	H_2 evolution	$56.3 \mu\text{mol h}^{-1}$ (AQY = 0.31% @ 400 nm)	[62]
	$\text{Au}_{2.0}/\text{TiO}_2/\text{CoO}$	CO_2 reduction to CH_4	$13.3 \mu\text{mol h}^{-1} \text{ g}^{-1}$	[103]
	Yolk-shell Au/TiO_2	Toluene degradation	57% removal in 180 min	[104]

4. Carbon Sphere Template Derived Hollow Nanostructure for Gas Sensing

Hollow nanostructure also has widely applied in gas sensing since it possesses ultrahigh specific area which can provide rich active sites for gas adsorption and diffusion, further promoting gas-sensing performance. Moreover, the porous structures resulting in high surface permeability also allows more gas exposure and makes gas sensing easier [105–107]. Inspired by carbon sphere templating methods in photocatalysis, researchers have successfully implemented the modification strategies into gas sensing in view of carbon spheres templated hollow nanostructure with adjustable composition, thickness, surface, and interface [108–110].

For instance, Zhang et al. [111] firstly designed porous $\text{Co}_3\text{O}_4/\text{Ta}_2\text{O}_5$ heterojunction hollow nanospheres. They prepared ultrathin Ta_2O_5 hollow shell (shell thickness ~ 5 nm) attached with numerous Co_3O_4 nanoparticles by adsorbing Co ions onto Ta^{5+}/C template spheres (Figure 20a–d). Figure 20e displayed that the gas sensor owned a good linear relationship of current vs. voltage between the sensing material and the electrode, ensuring that measured electrical signals were due to the gas-sensing performance rather than the contact resistance of the sensing material and the electrode. The gas sensor revealed splendid selectivity and reliable long stability to ethanol at room temperature (Figure 20h–k), which was attributed to two reasons: (1) the supporting effect of Ta_2O_5 hollow spheres hindered the agglomeration of Co_3O_4 particles and guaranteed larger BET area; (2) the formation of heterojunction resulted to widen the electronic depletion layer.

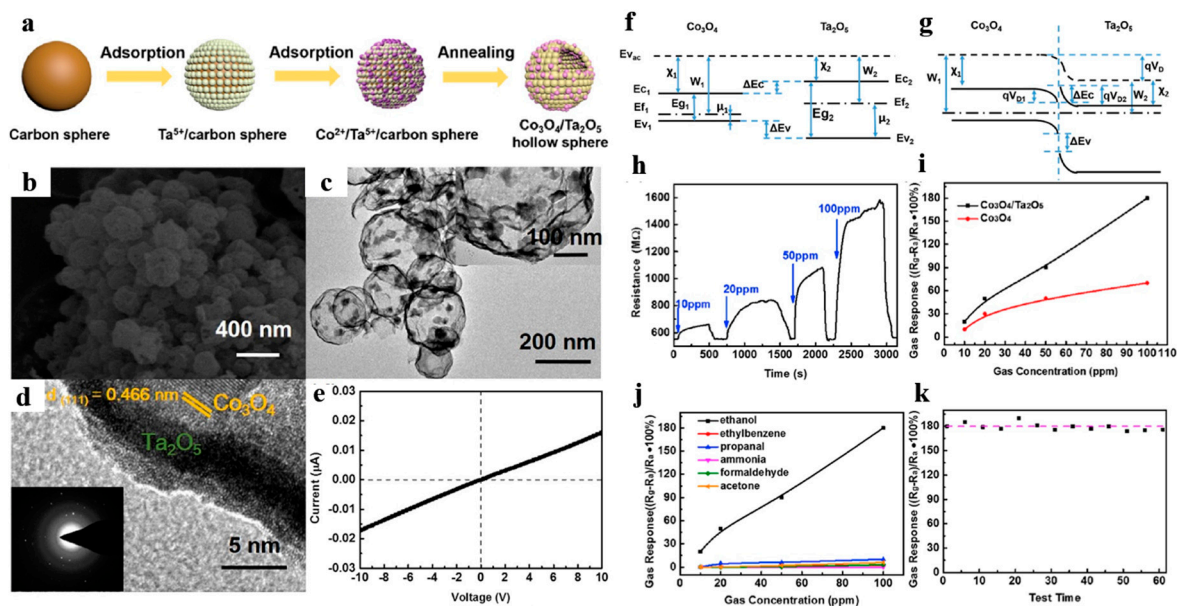


Figure 20. (a) Synthetic schematic of $\text{Co}_3\text{O}_4/\text{Ta}_2\text{O}_5$ heterostructure hollow nanospheres, (b) FESEM images, (c) TEM images, (d) HRTEM images. (e) I–V characteristics of the $\text{Co}_3\text{O}_4/\text{Ta}_2\text{O}_5$ sensor. Proposed energy band diagram: (f) before contact, (g) after contact. (h) Response and recovery curves of the $\text{Co}_3\text{O}_4/\text{Ta}_2\text{O}_5$ sensor at room temperature. (i) Sensitivity curves between the heterostructure and pure Co_3O_4 sensor with 10–100 ppm. (j) Selective test to several reducing gases with concentration of 10–100 ppm. (k) Long-term stability test during two months. Reproduced with permission from [111]. Copyright Elsevier, 2017.

Furthermore, Zhang et al. [112] also synthesized WO_3 mesoporous hollow nanospheres doped with Fe with a series of concentrations (0–5.2% by molar ratio) through a carbon colloidal nanosphere templating method, electrostatic adsorption of metal ions, as well as post-annealing treatment. This hollow structure showed tiny size and ultrahigh BET area. Gas sensor based on hollow nanostructured semiconductors finally realized outstanding performance applied for ppb-level NO_2 detection at lower working temperature (100–140 °C) as exhibited in Figure 21. According to the results of XPS, the enhancement of NO_2 detecting performance ascribed to rich oxygen vacancies and surface chemical states altered by Fe dopants. What is worth mentioning is that the excellent detection limitation can meet the needs of atmospheric monitoring and exclusive detecting at the same time.

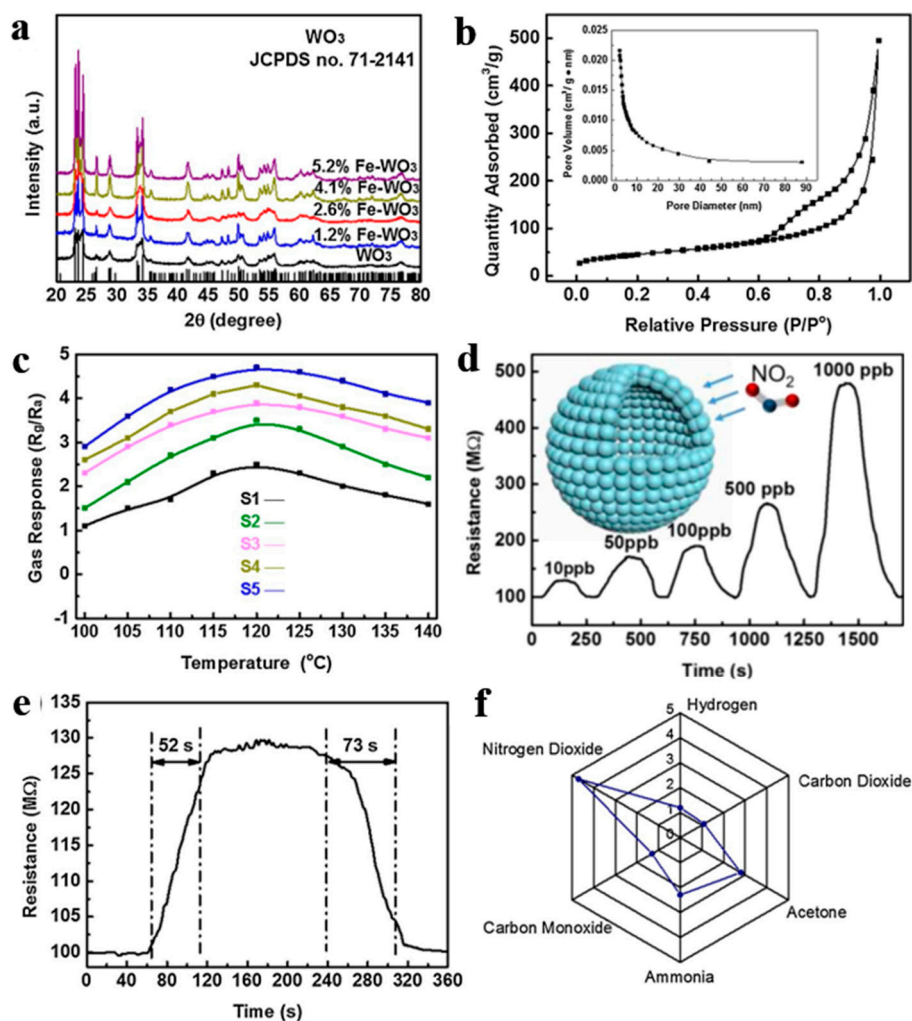


Figure 21. (a) XRD patterns. (b) N_2 adsorption and desorption isotherms and pore diameter distribution curves. (c) Response of all samples with different Fe doping contents from 100 to 140 °C to 1000 ppb NO_2 . The gas-sensing performance of the representative S5: (d) dynamic sensing curve to different NO_2 concentrations, (e) dynamic response curves to 10 ppb NO_2 at 120 °C, and (f) selective test to 1 ppm NO_2 versus several 10 ppm interfering gases. Reproduced with permission from [112]. Copyright Elsevier, 2018.

Zhang et al. [113] studied hollow carbon spheres of which Co_3O_4 nanowires assembled on the surface (Co_3O_4 NWs-HCSs) by hydrothermal method together with subsequent heat treatment for acetone gas sensing (Figure 22a). Obviously, Co_3O_4 NWs-HCSs behaved talented selectivity for acetone, and whose response increased to 23 at 150 °C, even possessed high response at lower temperature of 75 °C, approaching room temperature.

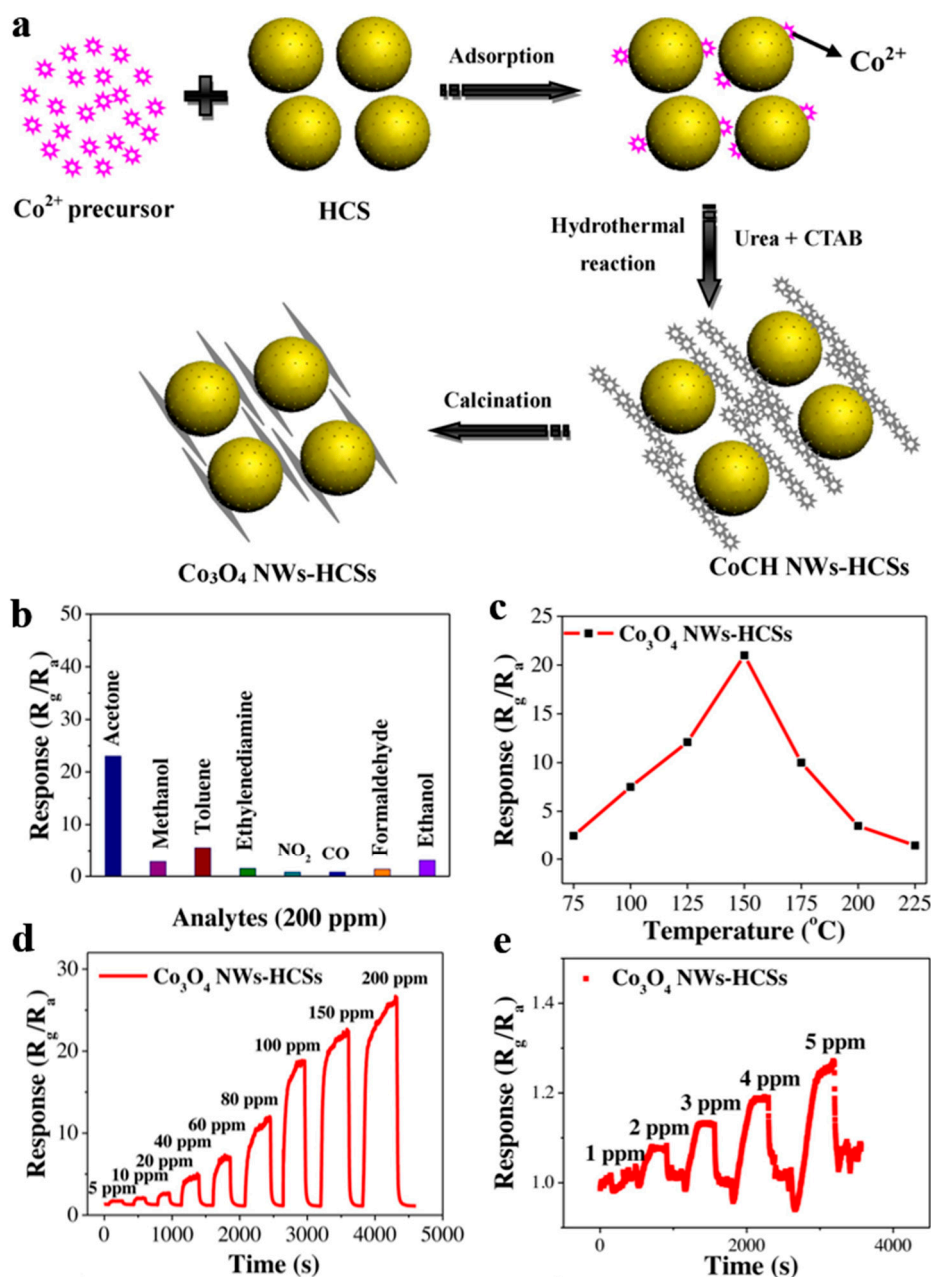


Figure 22. (a) Synthetic Schematic of Co_3O_4 NWs-HCSs. The gas-sensing performance of Co_3O_4 NWs-HCSs. (b) Sensing selectivity for several 200 ppm gases at 150 °C. (c) Sensing response versus operating temperature to 200 ppm acetone. (d,e) Dynamic sensing response to acetone within different concentration ranges at the operating temperature of 150 °C. Reproduced with permission from [113]. Copyright Elsevier, 2019.

Most researchers tend to study low temperature (even room temperature) and low concentration gas sensing taking the advantages of hollow structure, however they lacked research on humidity sensitivity. Notably, Mutuma et al. [114] reported that pristine hollow carbon spheres (HCSs), HCS/PVP (polyvinyl pyrrolidone) composite and annealed HCSs as ammonia sensors in damp conditions. The authors used a surfactant dispersion method to fabricate the HCSs and HCS/PVP. HCSs sensor should have responded in a high relative humidity (10–97% RH) owing to the presence of amorphous domains and oxygenated groups while high concentration of water molecules inhibited ammonia adsorption sites (Figure 23a). After adding PVP, HCSs still behaved obvious conductivity attenuation under high humidity resulting from polymer swelling and plasticization (Figure 23b). After subsequent

annealing, the annealed HCSs obtained a great response to 74–295 ppm NH_3 over a broad RH range (Figure 23c,h,i), decreasing the dependence on RH and raising surface area. This study provided insights into a step forward to modify the HCSs sensor in high humidity.

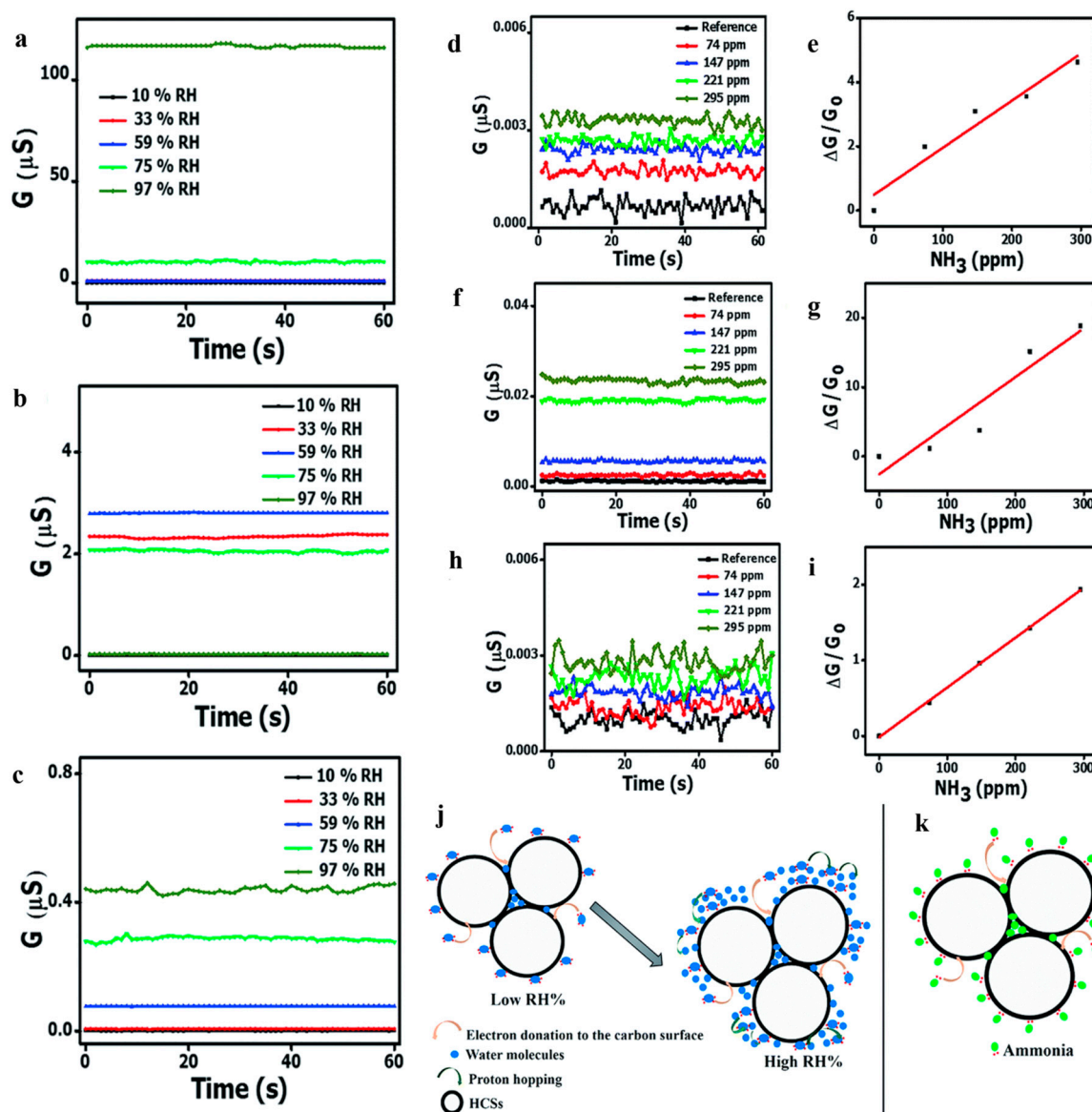


Figure 23. RH-dependent conductivity curves of (a) pure HCS, (b) HCS/PVP composite, and (c) annealed HCS based sensors at 40 °C. Ammonia concentration-dependent conductance and sensitivity of (d,e) pristine HCS, (f,g) HCS/PVP, and (h,i) annealed HCS based sensors at 10% RH at 40 °C. A schematic illustration of the sensing mechanism to NH_3 of the HCSs at low RH (j) and high RH (k). Reproduced with permission from [114]. Copyright Royal Society of Chemistry, 2017.

The above research presents several promising strategies to enhance gas-sensing performance through carbon sphere derived hollow nanostructure. Based on these studies, after further optimization on structure and process conditions, as well as material systems innovation, carbon sphere template derived hollow nanostructures would be promising in low temperature especially room temperature and ppb-level gas detection in high relative humidity environment, making it possible to apply in exhaled breath detecting in the future. A summary of the recent carbon sphere template derived hollow nanostructure gas sensors is presented in Table 2. Furthermore, hollow structures also have plenty of applications in the fields in energy storage [115,116].

Table 2. Summary of carbon sphere template derived hollow nanostructure for gas sensing.

Strategy	Material	Gas	Response	Reference
Doping	WO ₃ : C	acetone	5.1 @ 0.9 ppm, 300 °C	[109]
	WO ₃ : Fe	NO ₂	1.3 @ 10 ppb, 120 °C	[112]
Heterostructure	Pd@In ₂ O ₃	ethanol	159 @ 5 ppm, 350 °C	[108]
	Co ₃ O ₄ /Ta ₂ O ₅	ethanol	1.8 @ 100 ppm, 25 °C	[111]
	Co ₃ O ₄ @C	acetone	23 @ 200 ppm, 150 °C	[113]
Surface modification	Annealed C	ammonia	66 @ 74 ppm, 40 °C	[114]

5. Conclusion and Outlook

In summary, carbon sphere template derived hollow nanostructure has attracted considerable attention and achieved great progress in the fields of photocatalysis, gas sensing, etc. Among template methods, the use of highly hazardous, complex, inefficient, and costly fluoride-containing or strong acids and bases to etch the sacrificial templates limits their large-scale production and practical application. For these reasons, developing green, facile, and efficient strategies especially carbon sphere template derived hollow nanostructures with better photocatalysis and gas sensing performance is highly desirable and meaningful.

After tremendous efforts, the family of carbon sphere template derived hollow nanostructures have been broadened from monometal oxides to multimetal compounds. More importantly, doping, solid solution, heterostructure, and surface modification strategies have been successfully realized in carbon sphere template derived hollow nanostructures. These successful attempts are due to the unique characteristics of carbon sphere templates like the whole synthesis process is totally green and the surface radicals adsorb metal ions uniformly and non-selectively. This strategy is of great help to the three steps of photocatalytic process which enhancing light absorption, promoting carrier separation and benefiting surface redox reaction. This review summarized the recent development of carbon sphere template derived hollow nanostructures in photocatalysis. We summarize various synthetic routines of carbon spheres and carbon sphere template derived hollow nanostructures and highlight the mechanism for photocatalytic performance enhancement. The strategy has been also successfully applied in the field of gas sensing thus we present a summary of the recent progress in the development of carbon sphere template derived hollow nanostructures for gas sensing and related applications as well.

Despite significant progress in synthesis and effective property tuning of carbon sphere template derived hollow nanostructures, there are still some challenges and opportunities. For example, there are still many opportunities for research in the preparation of other types of fully adjustable solid solutions and tailoring bandgaps in most material systems. More systematic studies are needed to study the distribution of the minority atoms on the surface, such as whether the atomic dispersion can be achieved and applied to other reactions like photocatalytic CO₂ reduction or nitrogen fixation. It is important to realize synthesis of configurationally disordered and entropy-stabilized mixed metal oxides, especially consist of earth-abundant elements, using this uniformly and non-selectively adsorption method. Any progress in the above urgent problems, will make great contributions to their corresponding application fields. We hope this review can give an overview of the research progress in carbon sphere template derived hollow nanostructures, so that researchers can have a more in-depth understanding of the process and application of carbon sphere templating method, and we have given a brief description on the outlook of future development, so as to promote photocatalysis and gas sensing to practicality and benefit the development of scientific researches in these fields.

Author Contributions: Conceptualization, Z.L. and L.Z.; Investigation, Y.W. (Yichen Wang), Y.Y., Y.W. (Yanwen Wang), C.Q., R.L., and X.C.; Writing—original draft preparation, Y.W. (Yichen Wang); Writing—review and editing, Z.L.; Supervision, Z.Y. and L.Z.; Funding acquisition, Z.Y. and L.Z. All authors have read and agreed to the published version of the manuscript.

Funding: This research was funded by National Natural Science Foundation of China (51572239 and 91333203), Program for Innovative Research Team in University of Ministry of Education of China (IRT13037), the National Science and Technology Support Program (2012BAC08B08), and the Major Project of Zhejiang Natural Science Foundation of China (LD18E020002).

Conflicts of Interest: The authors declare no conflict of interest.

References

1. Gong, J.; Li, C.; Wasielewski, M.R. Advances in solar energy conversion. *Chem. Soc. Rev.* **2019**, *48*, 1862–1864. [[CrossRef](#)] [[PubMed](#)]
2. Fujishima, A.; Honda, K. Electrochemical photolysis of water at a semiconductor electrode. *Nature* **1972**, *238*, 37–38. [[CrossRef](#)] [[PubMed](#)]
3. Zou, Z.; Ye, J.; Sayama, K.; Arakawa, H. Direct splitting of water under visible light irradiation with an oxide semiconductor photocatalyst. *Nature* **2001**, *414*, 625–627. [[CrossRef](#)] [[PubMed](#)]
4. Yu, J.; Yu, X. Hydrothermal Synthesis and Photocatalytic Activity of Zinc Oxide Hollow Spheres. *Environ. Sci. Technol.* **2008**, *42*, 4902–4907. [[CrossRef](#)]
5. Song, H.; Meng, X.; Wang, Z.-j.; Wang, Z.; Chen, H.; Weng, Y.; Ichihara, F.; Oshikiri, M.; Kako, T.; Ye, J. Visible-Light-Mediated Methane Activation for Steam Methane Reforming under Mild Conditions: A Case Study of Rh/TiO₂ Catalysts. *ACS Catal.* **2018**, *8*, 7556–7565. [[CrossRef](#)]
6. Gyulavári, T.; Veréb, G.; Pap, Z.; Réti, B.; Baan, K.; Todea, M.; Magyari, K.; Szilágyi, M.I.; Hernadi, K. Utilization of Carbon Nanospheres in Photocatalyst Production: From Composites to Highly Active Hollow Structures. *Materials* **2019**, *12*, 2537. [[CrossRef](#)] [[PubMed](#)]
7. Wang, F.; Zhou, Y.; Pan, X.; Lu, B.; Huang, J.; Ye, Z. Enhanced photocatalytic properties of ZnO nanorods by electrostatic self-assembly with reduced graphene oxide. *Phys. Chem. Chem. Phys.* **2018**, *20*, 6959–6969. [[CrossRef](#)]
8. Niu, W.; Moehl, T.; Cui, W.; Wick-Joliat, R.; Zhu, L.; Tilley, S.D. Extended Light Harvesting with Dual Cu₂O-Based Photocathodes for High Efficiency Water Splitting. *Adv. Energy Mater.* **2018**, *8*, 1702323. [[CrossRef](#)]
9. Song, H.; Meng, X.; Wang, S.; Zhou, W.; Wang, X.; Kako, T.; Ye, J. Direct and Selective Photocatalytic Oxidation of CH₄ to Oxygenates with O₂ on Cocatalysts/ZnO at Room Temperature in Water. *J. Am. Chem. Soc.* **2019**, *141*, 20507–20515. [[CrossRef](#)]
10. Maeda, K.; Domen, K. New Non-Oxide Photocatalysts Designed for Overall Water Splitting under Visible Light. *J. Phys. Chem. C* **2007**, *111*, 7851–7861. [[CrossRef](#)]
11. Li, Q.; Guo, B.; Yu, J.; Ran, J.; Zhang, B.; Yan, H.; Gong, J.R. Highly efficient visible-light-driven photocatalytic hydrogen production of CdS-cluster-decorated graphene nanosheets. *J. Am. Chem. Soc.* **2011**, *133*, 10878–10884. [[CrossRef](#)] [[PubMed](#)]
12. Zong, X.; Yan, H.; Wu, G.; Ma, G.; Wen, F.; Wang, L.; Li, C. Enhancement of Photocatalytic H₂ Evolution on CdS by Loading MoS₂ as Cocatalyst under Visible Light Irradiation. *J. Am. Chem. Soc.* **2008**, *130*, 7176–7177. [[CrossRef](#)] [[PubMed](#)]
13. Zhang, J.; Yu, J.; Jaroniec, M.; Gong, J.R. Noble Metal-Free Reduced Graphene Oxide-Zn_xCd_{1-x}S Nanocomposite with Enhanced Solar Photocatalytic H₂-Production Performance. *Nano Lett.* **2012**, *12*, 4584–4589. [[CrossRef](#)] [[PubMed](#)]
14. Zhang, Z.; Shao, C.; Li, X.; Sun, Y.; Zhang, M.; Mu, J.; Zhang, P.; Guo, Z.; Liu, Y. Hierarchical assembly of ultrathin hexagonal SnS₂ nanosheets onto electrospun TiO₂ nanofibers: Enhanced photocatalytic activity based on photoinduced interfacial charge transfer. *Nanoscale* **2013**, *5*, 606–618. [[CrossRef](#)]
15. Khazaei, M.; Arai, M.; Sasaki, T.; Chung, C.-Y.; Venkataramanan, N.S.; Estili, M.; Sakka, Y.; Kawazoe, Y. Novel Electronic and Magnetic Properties of Two-Dimensional Transition Metal Carbides and Nitrides. *Adv. Funct. Mater.* **2013**, *23*, 2185–2192. [[CrossRef](#)]
16. Cao, S.; Low, J.; Yu, J.; Jaroniec, M. Polymeric Photocatalysts Based on Graphitic Carbon Nitride. *Adv. Mater.* **2015**, *27*, 2150–2176. [[CrossRef](#)] [[PubMed](#)]
17. Hara, M.; Hitoki, G.; Takata, T.; Kondo, J.N.; Kobayashi, H.; Domen, K. TaON and Ta₃N₅ as new visible light driven photocatalysts. *Catal. Today* **2003**, *78*, 555–560. [[CrossRef](#)]

18. Yang, Y.; Lou, Z.; Lei, W.; Wang, Y.; Liang, R.; Qin, C.; Zhu, L. Enhanced photoelectrochemical water-splitting performance of SrNbO₂N photoanodes using flux-assisted synthesis method and surface defect management. *Sustain. Energy Fuels* **2020**. [[CrossRef](#)]
19. Liu, J.; Wen, S.; Hou, Y.; Zuo, F.; Beran, G.J.O.; Feng, P. Boron Carbides as Efficient, Metal-Free, Visible-Light-Responsive Photocatalysts. *Angew. Chem. Int. Ed.* **2013**, *52*, 3241–3245. [[CrossRef](#)]
20. Vrubel, H.; Hu, X. Molybdenum Boride and Carbide Catalyze Hydrogen Evolution in both Acidic and Basic Solutions. *Angew. Chem. Int. Ed.* **2012**, *51*, 12703–12706. [[CrossRef](#)]
21. Garcia-Esparza, A.T.; Cha, D.; Ou, Y.; Kubota, J.; Domen, K.; Takanabe, K. Tungsten Carbide Nanoparticles as Efficient Cocatalysts for Photocatalytic Overall Water Splitting. *ChemSusChem* **2013**, *6*, 168–181. [[CrossRef](#)] [[PubMed](#)]
22. Goto, Y.; Hisatomi, T.; Wang, Q.; Higashi, T.; Ishikiriyama, K.; Maeda, T.; Sakata, Y.; Okunaka, S.; Tokudome, H.; Katayama, M.; et al. A Particulate Photocatalyst Water-Splitting Panel for Large-Scale Solar Hydrogen Generation. *Joule* **2018**, *2*, 509–520. [[CrossRef](#)]
23. Wang, Q.; Okunaka, S.; Tokudome, H.; Hisatomi, T.; Nakabayashi, M.; Shibata, N.; Yamada, T.; Domen, K. Printable Photocatalyst Sheets Incorporating a Transparent Conductive Mediator for Z-Scheme Water Splitting. *Joule* **2018**, *2*, 2667–2680. [[CrossRef](#)]
24. Wang, Q.; Hisatomi, T.; Jia, Q.; Tokudome, H.; Zhong, M.; Wang, C.; Pan, Z.; Takata, T.; Nakabayashi, M.; Shibata, N.; et al. Scalable water splitting on particulate photocatalyst sheets with a solar-to-hydrogen energy conversion efficiency exceeding 1%. *Nat. Mater.* **2016**, *15*, 611–615. [[CrossRef](#)] [[PubMed](#)]
25. Moniz, S.J.A.; Shevlin, S.A.; Martin, D.J.; Guo, Z.-X.; Tang, J. Visible-light driven heterojunction photocatalysts for water splitting—A critical review. *Energy Environ. Sci.* **2015**, *8*, 731–759. [[CrossRef](#)]
26. Lewis, N.S. Light work with water. *Nature* **2001**, *414*, 589–590. [[CrossRef](#)] [[PubMed](#)]
27. Sabio, E.M.; Chamousis, R.L.; Browning, N.D.; Osterloh, F.E. Photocatalytic Water Splitting with Suspended Calcium Niobium Oxides: Why Nanoscale is Better than Bulk—A Kinetic Analysis. *J. Phys. Chem. C* **2012**, *116*, 3161–3170. [[CrossRef](#)]
28. Li, L.; Yan, J.; Wang, T.; Zhao, Z.J.; Zhang, J.; Gong, J.; Guan, N. Sub-10 nm rutile titanium dioxide nanoparticles for efficient visible-light-driven photocatalytic hydrogen production. *Nat. Commun.* **2015**, *6*, 5881. [[CrossRef](#)]
29. Deshmukh, A.A.; Mhlanga, S.D.; Coville, N.J. Carbon spheres. *Mater. Sci. Eng. R* **2010**, *70*, 1–28. [[CrossRef](#)]
30. Zhang, Y.; Yang, W.; Luo, R.-y.; Shang, H.-d. Preparation of carbon nanospheres by non-catalytic chemical vapor deposition and their formation mechanism. *New Carbon Mater.* **2016**, *31*, 467–474. [[CrossRef](#)]
31. Zhao, X.; Li, W.; Zhang, S.; Liu, L.; Liu, S. Facile fabrication of hollow and honeycomb-like carbon spheres from liquefied larch sawdust via ultrasonic spray pyrolysis. *Mater. Lett.* **2015**, *157*, 135–138. [[CrossRef](#)]
32. Sun, X.; Li, Y. Colloidal carbon spheres and their core/shell structures with noble-metal nanoparticles. *Angew. Chem. Int. Ed.* **2004**, *43*, 597–601. [[CrossRef](#)] [[PubMed](#)]
33. Sun, X.; Li, Y. Ga₂O₃ and GaN semiconductor hollow spheres. *Angew. Chem. Int. Ed.* **2004**, *43*, 3827–3831. [[CrossRef](#)] [[PubMed](#)]
34. Wang, Q.; Li, H.; Chen, L.Q.; Huang, X.J. Monodispersed hard carbon spherules with uniform nanopores. *Carbon* **2001**, *39*, 2211–2214. [[CrossRef](#)]
35. Titirici, M.-M.; Antonietti, M.; Thomas, A. A Generalized Synthesis of Metal Oxide Hollow Spheres Using a Hydrothermal Approach. *Chem. Mater.* **2006**, *18*, 3808–3812. [[CrossRef](#)]
36. Tan, Y.; Liu, M.; Wei, D.; Tang, H.; Feng, X.; Shen, S. A simple green approach to synthesis of sub-100 nm carbon spheres as template for TiO₂ hollow nanospheres with enhanced photocatalytic activities. *Sci. China Mater.* **2018**, *61*, 869–877. [[CrossRef](#)]
37. Wang, X.; Feng, J.; Bai, Y.; Zhang, Q.; Yin, Y. Synthesis, Properties, and Applications of Hollow Micro-/Nanostructures. *Chem. Rev.* **2016**, *116*, 10983–11060. [[CrossRef](#)]
38. Yan, Q.; Li, R.; Toghiani, H.; Cai, Z.; Zhang, J. Synthesis and Characterization of Carbon Nanospheres Obtained by Hydrothermal Carbonization of Wood-derived and Other Saccharides. *Trends Renew. Energy* **2015**, *1*, 119. [[CrossRef](#)]
39. Aydıncak, K.; Yumak, T.; Sinağ, A.; Esen, B. Synthesis and Characterization of Carbonaceous Materials from Saccharides (Glucose and Lactose) and Two Waste Biomasses by Hydrothermal Carbonization. *Ind. Eng. Chem. Res.* **2012**, *51*, 9145–9152. [[CrossRef](#)]

40. Zheng, M.T.; Liu, Y.L.; Xiao, Y.; Zhu, Y.; Guan, Q.; Yuan, D.S.; Zhang, J.X. An Easy Catalyst-Free Hydrothermal Method to Prepare Monodisperse Carbon Microspheres on a Large Scale. *J. Phys. Chem. C* **2009**, *113*, 8455–8459. [[CrossRef](#)]
41. Yu, L.; Falco, C.; Weber, J.; White, R.J.; Howe, J.Y.; Titirici, M.M. Carbohydrate-derived hydrothermal carbons: A thorough characterization study. *Langmuir* **2012**, *28*, 12373–12383. [[CrossRef](#)] [[PubMed](#)]
42. Sevilla, M.; Fuertes, A.B. The production of carbon materials by hydrothermal carbonization of cellulose. *Carbon* **2009**, *47*, 2281–2289. [[CrossRef](#)]
43. Gong, J.; Liu, J.; Chen, X.; Wen, X.; Jiang, Z.; Mijowska, E.; Wang, Y.; Tang, T. Synthesis, characterization and growth mechanism of mesoporous hollow carbon nanospheres by catalytic carbonization of polystyrene. *Microporous Mesoporous Mater.* **2013**, *176*, 31–40. [[CrossRef](#)]
44. Li, S.; Pasc, A.; Fierro, V.; Celzard, A. Hollow carbon spheres, synthesis and applications—A review. *J. Mater. Chem. A* **2016**, *4*, 12686–12713. [[CrossRef](#)]
45. Ji, L.; Qiao, W.; Huang, K.; Zhang, Y.; Wu, H.; Miao, S.; Liu, H.; Dong, Y.; Zhu, A.; Qiu, D. Synthesis of nanosized 58S bioactive glass particles by a three-dimensional ordered macroporous carbon template. *Mater. Sci. Eng. C* **2017**, *75*, 590–595. [[CrossRef](#)] [[PubMed](#)]
46. Smith, S.J.; Huang, B.; Liu, S.; Liu, Q.; Olsen, R.E.; Boerio-Goates, J.; Woodfield, B.F. Synthesis of metal oxide nanoparticles via a robust “solvent-deficient” method. *Nanoscale* **2015**, *7*, 144–156. [[CrossRef](#)]
47. Wu, H.; Wu, G.; Ren, Y.; Li, X.; Wang, L. Multishelled Metal Oxide Hollow Spheres: Easy Synthesis and Formation Mechanism. *Chem.-Eur. J.* **2016**, *22*, 8864–8871. [[CrossRef](#)]
48. Marschall, R.; Wang, L. Non-metal doping of transition metal oxides for visible-light photocatalysis. *Catal. Today* **2014**, *225*, 111–135. [[CrossRef](#)]
49. Wang, S.; Yun, J.-H.; Luo, B.; Butburee, T.; Peerakiatkhajohn, P.; Thaweesak, S.; Xiao, M.; Wang, L. Recent Progress on Visible Light Responsive Heterojunctions for Photocatalytic Applications. *J. Mater. Sci. Technol.* **2017**, *33*, 1–22. [[CrossRef](#)]
50. Gu, X.; Yuan, S.; Ma, M.; Zhu, J. Nanoenhanced Materials for Photolytic Hydrogen Production. *Nanotechnol. Energy Sustain.* **2017**, 629. [[CrossRef](#)]
51. Lee, G.-J.; Wu, J.J. Recent developments in ZnS photocatalysts from synthesis to photocatalytic applications—A review. *Powder Technol.* **2017**, *318*, 8–22. [[CrossRef](#)]
52. Song, H.; Li, Y.; Lou, Z.; Xiao, M.; Hu, L.; Ye, Z.; Zhu, L. Synthesis of Fe-doped WO₃ nanostructures with high visible-light-driven photocatalytic activities. *Appl. Catal. B-Environ.* **2015**, *166–167*, 112–120. [[CrossRef](#)]
53. Wu, Z.; Li, Y.; Gao, L.; Wang, S.; Fu, G. Synthesis of Na-doped ZnO hollow spheres with improved photocatalytic activity for hydrogen production. *Dalton Trans.* **2016**, *45*, 11145–11149. [[CrossRef](#)] [[PubMed](#)]
54. Wang, C.; Ao, Y.; Wang, P.; Hou, J.; Qian, J. Preparation, characterization and photocatalytic activity of the neodymium-doped TiO₂ hollow spheres. *Appl. Surf. Sci.* **2010**, *257*, 227–231. [[CrossRef](#)]
55. Wang, C.; Ao, Y.; Wang, P.; Hou, J.; Qian, J.; Zhang, S. Preparation, characterization, photocatalytic properties of titania hollow sphere doped with cerium. *J. Hazard. Mater.* **2010**, *178*, 517–521. [[CrossRef](#)]
56. Shi, J.-W.; Zong, X.; Wu, X.; Cui, H.-J.; Xu, B.; Wang, L.; Fu, M.-L. Carbon-doped Titania Hollow Spheres with Tunable Hierarchical Macroporous Channels and Enhanced Visible Light-induced Photocatalytic Activity. *ChemCatChem* **2012**, *4*, 488–491. [[CrossRef](#)]
57. Shi, J.-W.; Chen, J.-W.; Cui, H.-J.; Fu, M.-L.; Luo, H.-Y.; Xu, B.; Ye, Z.-L. One template approach to synthesize C-doped titania hollow spheres with high visible-light photocatalytic activity. *Chem. Eng. J.* **2012**, *195–196*, 226–232. [[CrossRef](#)]
58. Zou, Y.; Shi, J.-W.; Ma, D.; Fan, Z.; Lu, L.; Niu, C. In situ synthesis of C-doped TiO₂@g-C₃N₄ core-shell hollow nanospheres with enhanced visible-light photocatalytic activity for H₂ evolution. *Chem. Eng. J.* **2017**, *322*, 435–444. [[CrossRef](#)]
59. Wang, Q.; Zhu, S.; Liang, Y.; Cui, Z.; Yang, X.; Liang, C.; Inoue, A. Synthesis of Br-doped TiO₂ hollow spheres with enhanced photocatalytic activity. *J. Nanopart. Res.* **2017**, *19*, 72. [[CrossRef](#)]
60. Li, Y.; Li, F.; Li, X.; Song, H.; Lou, Z.; Ye, Z.; Zhu, L. Ultrahigh efficient water oxidation under visible light: Using Fe dopants to integrate nanostructure and cocatalyst in LaTiO₂N system. *Nano Energy* **2016**, *19*, 437–445. [[CrossRef](#)]
61. Gao, L.; Li, Y.; Ren, J.; Wang, S.; Wang, R.; Fu, G.; Hu, Y. Passivation of defect states in anatase TiO₂ hollow spheres with Mg doping: Realizing efficient photocatalytic overall water splitting. *Appl. Catal. B-Environ.* **2017**, *202*, 127–133. [[CrossRef](#)]

62. Xiao, M.; Wang, Z.; Luo, B.; Wang, S.; Wang, L. Enhancing photocatalytic activity of tantalum nitride by rational suppression of bulk, interface and surface charge recombination. *Appl. Catal. B-Environ.* **2019**, *246*, 195–201. [[CrossRef](#)]
63. Liu, B.; Li, J.; Yang, W.; Zhang, X.; Jiang, X.; Bando, Y. Semiconductor Solid-Solution Nanostructures: Synthesis, Property Tailoring, and Applications. *Small* **2017**, *13*, 1701998. [[CrossRef](#)] [[PubMed](#)]
64. Tsuji, I.; Kato, H.; Kobayashi, H.; Kudo, A. Photocatalytic H₂ evolution reaction from aqueous solutions over band structure-controlled (AgIn)_xZn_{2(1-x)}S₂ solid solution photocatalysts with visible-light response and their surface nanostructures. *J. Am. Chem. Soc.* **2004**, *126*, 13406–13413. [[CrossRef](#)]
65. Maeda, K.; Takata, T.; Hara, M.; Saito, N.; Inoue, Y.; Kobayashi, H.; Domen, K. GaN:ZnO solid solution as a photocatalyst for visible-light-driven overall water splitting. *J. Am. Chem. Soc.* **2005**, *127*, 8286–8287. [[CrossRef](#)]
66. Wei, S.; Zunger, A. Role of metal d states in II-VI semiconductors. *Phys. Rev. B* **1988**, *37*, 8958–8981. [[CrossRef](#)]
67. Maeda, K.; Teramura, K.; Domen, K. Effect of post-calcination on photocatalytic activity of (Ga_{1-x}Zn_x)(N_{1-x}O_x) solid solution for overall water splitting under visible light. *J. Catal.* **2008**, *254*, 198–204. [[CrossRef](#)]
68. Reinert, A.A.; Payne, C.; Wang, L.; Ciston, J.; Zhu, Y.; Khalifah, P.G. Synthesis and characterization of visible light absorbing (GaN)_(1-x)(ZnO)_x semiconductor nanorods. *Inorg. Chem.* **2013**, *52*, 8389–8398. [[CrossRef](#)]
69. Li, Y.; Zhu, L.; Yang, Y.; Song, H.; Lou, Z.; Guo, Y.; Ye, Z. A full compositional range for a (Ga_{1-x}Zn_x)(N_{1-x}O_x) nanostructure: High efficiency for overall water splitting and optical properties. *Small* **2015**, *11*, 871–876. [[CrossRef](#)]
70. Kamata, K.; Maeda, K.; Lu, D.; Kako, Y.; Domen, K. Synthesis and photocatalytic activity of gallium–zinc–indium mixed oxynitride for hydrogen and oxygen evolution under visible light. *Chem. Phys. Lett.* **2009**, *470*, 90–94. [[CrossRef](#)]
71. Mei, Z.; Zhang, M.; Schneider, J.; Wang, W.; Zhang, N.; Su, Y.; Chen, B.; Wang, S.; Rogach, A.L.; Pan, F. Hexagonal Zn_{1-x}Cd_xS (0.2 ≤ x ≤ 1) solid solution photocatalysts for H₂ generation from water. *Catal. Sci. Technol.* **2017**, *7*, 982–987. [[CrossRef](#)]
72. Shen, C.-C.; Liu, Y.-N.; Zhou, X.; Guo, H.-L.; Zhao, Z.-W.; Liang, K.; Xu, A.-W. Large improvement of visible-light photocatalytic H₂-evolution based on cocatalyst-free Zn_{0.5}Cd_{0.5}S synthesized through a two-step process. *Catal. Sci. Technol.* **2017**, *7*, 961–967. [[CrossRef](#)]
73. Gholipour, M.R.; Nguyen, C.C.; Béland, F.; Do, T.-O. Hollow microspheres consisting of uniform Zn_xCd_{1-x}S nanoparticles with noble-metal-free co-catalysts for hydrogen evolution with high quantum efficiency under visible light. *J. Photochem. Photobiol. A-Chem.* **2018**, *358*, 1–9. [[CrossRef](#)]
74. Shen, L.; Yu, L.; Wu, H.B.; Yu, X.Y.; Zhang, X.; Lou, X.W. Formation of nickel cobalt sulfide ball-in-ball hollow spheres with enhanced electrochemical pseudocapacitive properties. *Nat. Commun.* **2015**, *6*, 6694. [[CrossRef](#)]
75. Nguyen, C.C.; Vu, N.N.; Do, T.-O. Recent advances in the development of sunlight-driven hollow structure photocatalysts and their applications. *J. Mater. Chem. A* **2015**, *3*, 18345–18359. [[CrossRef](#)]
76. Zhang, P.; Lou, X.W.D. Design of Heterostructured Hollow Photocatalysts for Solar-to-Chemical Energy Conversion. *Adv. Mater.* **2019**, *31*, 1900281. [[CrossRef](#)]
77. Xiao, M.; Wang, Z.; Lyu, M.; Luo, B.; Wang, S.; Liu, G.; Cheng, H.M.; Wang, L. Hollow Nanostructures for Photocatalysis: Advantages and Challenges. *Adv. Mater.* **2018**, *31*, 1801369. [[CrossRef](#)]
78. Low, J.; Yu, J.; Jaroniec, M.; Wageh, S.; Al-Ghamdi, A.A. Heterojunction Photocatalysts. *Adv. Mater.* **2017**, *29*, 1601694. [[CrossRef](#)]
79. Sivula, K. Toward Economically Feasible Direct Solar-to-Fuel Energy Conversion. *J. Phys. Chem. Lett.* **2015**, *6*, 975–976. [[CrossRef](#)]
80. Song, H.; Zhu, L.; Li, Y.; Lou, Z.; Xiao, M.; Ye, Z. Preparation of ZnFe₂O₄ nanostructures and highly efficient visible-light-driven hydrogen generation with the assistance of nanoheterostructures. *J. Mater. Chem. A* **2015**, *3*, 8353–8360. [[CrossRef](#)]
81. Li, C.; Lou, Z.; Yang, Y.; Wang, Y.; Lu, Y.; Ye, Z.; Zhu, L. Hollowsphere Nanoheterojunction of g-C₃N₄@TiO₂ with High Visible Light Photocatalytic Property. *Langmuir* **2019**, *35*, 779–786. [[CrossRef](#)]
82. Lou, Z.; Li, Y.; Zhu, L.; Xie, W.; Niu, W.; Song, H.; Ye, Z.; Zhang, S. The crystalline/amorphous contact in Cu₂O/Ta₂O₅ heterostructures: Increasing its sunlight-driven overall water splitting efficiency. *J. Mater. Chem. A* **2017**, *5*, 2732–2738. [[CrossRef](#)]
83. Waqas, M.; Wei, Y.; Mao, D.; Qi, J.; Yang, Y.; Wang, B.; Wang, D. Multi-shelled TiO₂/Fe₂TiO₅ heterostructured hollow microspheres for enhanced solar water oxidation. *Nano Res.* **2017**, *10*, 3920–3928. [[CrossRef](#)]

84. Dai, F.; Zhao, R.; Huai, X.; Han, J.; Wang, L.; Feng, S. Magnetic ZnFe₂O₄@ZnSe hollow nanospheres for photocatalytic hydrogen production application. *Compos. Part B-Eng.* **2019**, *173*, 106891. [[CrossRef](#)]
85. Ang, J.K.K.; Juay, J.; Kok, Y.H.; Bai, H.; Sun, D.D. Multi-dimensional micro-/nano-reactor spheres for sustainable water treatment. *Catal. Sci. Technol.* **2017**, *7*, 5550–5561. [[CrossRef](#)]
86. Li, Y.; Zhu, L.; Guo, Y.; Song, H.; Lou, Z.; Ye, Z. A new type of hybrid nanostructure: Complete photo-generated carrier separation and ultrahigh photocatalytic activity. *J. Mater. Chem. A* **2014**, *2*, 14245–14250. [[CrossRef](#)]
87. Lou, Z.; Li, Y.; Song, H.; Ye, Z.; Zhu, L. Fabrication of Fe₂TiO₅/TiO₂ nanoheterostructures with enhanced visible-light photocatalytic activity. *RSC Adv.* **2016**, *6*, 45343–45348. [[CrossRef](#)]
88. Liu, Y.; Yu, L.; Hu, Y.; Guo, C.; Zhang, F.; Wen David Lou, X. A magnetically separable photocatalyst based on nest-like γ -Fe₂O₃/ZnO double-shelled hollow structures with enhanced photocatalytic activity. *Nanoscale* **2012**, *4*, 183–187. [[CrossRef](#)] [[PubMed](#)]
89. Zhang, L.; Zhang, J.; Jiu, H.; Zhang, X.; Xu, M. Preparation of hollow core/shell CeO₂@TiO₂ with enhanced photocatalytic performance. *J. Mater. Sci.* **2015**, *50*, 5228–5237. [[CrossRef](#)]
90. Lv, K.; Li, J.; Qing, X.; Li, W.; Chen, Q. Synthesis and photo-degradation application of WO₃/TiO₂ hollow spheres. *J. Hazard. Mater.* **2011**, *189*, 329–335. [[CrossRef](#)]
91. Zhang, C.; Yin, L.; Zhang, L.; Qi, Y.; Lun, N. Preparation and photocatalytic activity of hollow ZnO and ZnO–CuO composite spheres. *Mater. Lett.* **2012**, *67*, 303–307. [[CrossRef](#)]
92. Jin, C.; Ge, C.; Jian, Z.; Wei, Y. Facile Synthesis and High Photocatalytic Degradation Performance of ZnO–SnO₂ Hollow Spheres. *Nanoscale Res. Lett.* **2016**, *11*, 526. [[CrossRef](#)] [[PubMed](#)]
93. Zou, Z.; Yang, X.; Zhang, P.; Zhang, Y.; Yan, X.; Zhou, R.; Liu, D.; Xu, L.; Gui, J. Trace carbon-hybridized ZnS/ZnO hollow nanospheres with multi-enhanced visible-light photocatalytic performance. *J. Alloys Compd.* **2019**, *775*, 481–489. [[CrossRef](#)]
94. Matsukawa, M.; Ishikawa, R.; Hisatomi, T.; Moriya, Y.; Shibata, N.; Kubota, J.; Ikuhara, Y.; Domen, K. Enhancing photocatalytic activity of LaTiO₂N by removal of surface reconstruction layer. *Nano Lett.* **2014**, *14*, 1038–1041. [[CrossRef](#)] [[PubMed](#)]
95. Li, Y.; Cheng, X.; Ruan, X.; Song, H.; Lou, Z.; Ye, Z.; Zhu, L. Enhancing photocatalytic activity for visible-light-driven H₂ generation with the surface reconstructed LaTiO₂N nanostructures. *Nano Energy* **2015**, *12*, 775–784. [[CrossRef](#)]
96. Chen, X.; Liu, L.; Yu, P.Y.; Mao, S.S. Increasing solar absorption for photocatalysis with black hydrogenated titanium dioxide nanocrystals. *Science* **2011**, *331*, 746–750. [[CrossRef](#)]
97. Thompson, T.L.; Yates, J.T., Jr. Surface science studies of the photoactivation of TiO₂—new photochemical processes. *Chem. Rev.* **2006**, *106*, 4428–4453. [[CrossRef](#)]
98. Pan, X.; Yang, M.Q.; Fu, X.; Zhang, N.; Xu, Y.J. Defective TiO₂ with oxygen vacancies: Synthesis, properties and photocatalytic applications. *Nanoscale* **2013**, *5*, 3601–3614. [[CrossRef](#)]
99. Chen, X.; Liu, L.; Huang, F. Black titanium dioxide (TiO₂) nanomaterials. *Chem. Soc. Rev.* **2015**, *44*, 1861–1885. [[CrossRef](#)]
100. Song, H.; Li, C.X.; Lou, Z.R.; Ye, Z.Z.; Zhu, L.P. Effective Formation of Oxygen Vacancies in Black TiO₂ Nanostructures with Efficient Solar-Driven Water Splitting. *ACS Sustain. Chem. Eng.* **2017**, *5*, 8982–8987. [[CrossRef](#)]
101. Ng, Y.H.; Ikeda, S.; Matsumura, M.; Amal, R. A perspective on fabricating carbon-based nanomaterials by photocatalysis and their applications. *Energy Environ. Sci.* **2012**, *5*, 9307–9318. [[CrossRef](#)]
102. Li, A.; Wang, T.; Chang, X.; Cai, W.; Zhang, P.; Zhang, J.; Gong, J. Spatial separation of oxidation and reduction co-catalysts for efficient charge separation: Pt@TiO₂@MnO_x hollow spheres for photocatalytic reactions. *Chem. Sci.* **2016**, *7*, 890–895. [[CrossRef](#)] [[PubMed](#)]
103. Zhu, S.; Liao, W.; Zhang, M.; Liang, S. Design of spatially separated Au and CoO dual cocatalysts on hollow TiO₂ for enhanced photocatalytic activity towards the reduction of CO₂ to CH₄. *Chem. Eng. J.* **2019**, *361*, 461–469. [[CrossRef](#)]
104. Wang, Y.; Yang, C.; Chen, A.; Pu, W.; Gong, J. Influence of yolk-shell Au@TiO₂ structure induced photocatalytic activity towards gaseous pollutant degradation under visible light. *Appl. Catal. B-Environ.* **2019**, *251*, 57–65. [[CrossRef](#)]
105. Drobek, M.; Kim, J.H.; Bechelany, M.; Vallicari, C.; Julbe, A.; Kim, S.S. MOF-Based Membrane Encapsulated ZnO Nanowires for Enhanced Gas Sensor Selectivity. *ACS Appl. Mater. Interfaces* **2016**, *8*, 8323–8328. [[CrossRef](#)]

106. Qu, F.; Jiang, H.; Yang, M. Designed formation through a metal organic framework route of ZnO/ZnCo₂O₄ hollow core-shell nanocages with enhanced gas sensing properties. *Nanoscale* **2016**, *8*, 16349–16356. [[CrossRef](#)] [[PubMed](#)]
107. Wang, X.; Zhang, S.; Shao, M.; Huang, J.; Deng, X.; Hou, P.; Xu, X. Fabrication of ZnO/ZnFe₂O₄ hollow nanocages through metal organic frameworks route with enhanced gas sensing properties. *Sens. Actuator B-Chem.* **2017**, *251*, 27–33. [[CrossRef](#)]
108. Rai, P.; Yoon, J.-W.; Kwak, C.-H.; Lee, J.-H. Role of Pd nanoparticles in gas sensing behaviour of Pd@In₂O₃ yolk-shell nanoreactors. *J. Mater. Chem. A* **2016**, *4*, 264–269. [[CrossRef](#)]
109. Shen, J.-Y.; Zhang, L.; Ren, J.; Wang, J.-C.; Yao, H.-C.; Li, Z.-J. Highly enhanced acetone sensing performance of porous C-doped WO₃ hollow spheres by carbon spheres as templates. *Sens. Actuator B-Chem.* **2017**, *239*, 597–607. [[CrossRef](#)]
110. Yang, H.M.; Ma, S.Y.; Jiao, H.Y.; Chen, Q.; Lu, Y.; Jin, W.X.; Li, W.Q.; Wang, T.T.; Jiang, X.H.; Qiang, Z.; et al. Synthesis of Zn₂SnO₄ hollow spheres by a template route for high-performance acetone gas sensor. *Sens. Actuator B-Chem.* **2017**, *245*, 493–506. [[CrossRef](#)]
111. Zhang, Z.; Wen, Z.; Ye, Z.; Zhu, L. Synthesis of Co₃O₄/Ta₂O₅ heterostructure hollow nanospheres for enhanced room temperature ethanol gas sensor. *J. Alloys Compd.* **2017**, *727*, 436–443. [[CrossRef](#)]
112. Zhang, Z.; Haq, M.; Wen, Z.; Ye, Z.; Zhu, L. Ultrasensitive ppb-level NO₂ gas sensor based on WO₃ hollow nanospheres doped with Fe. *Appl. Surf. Sci.* **2018**, *434*, 891–897. [[CrossRef](#)]
113. Zhang, C.; Li, L.; Hou, L.; Chen, W. Fabrication of Co₃O₄ nanowires assembled on the surface of hollow carbon spheres for acetone gas sensing. *Sens. Actuator B-Chem.* **2019**, *291*, 130–140. [[CrossRef](#)]
114. Mutuma, B.K.; Rodrigues, R.; Ranganathan, K.; Matsoso, B.; Wamwangi, D.; Hümmelgen, I.A.; Coville, N.J. Hollow carbon spheres and a hollow carbon sphere/polyvinylpyrrolidone composite as ammonia sensors. *J. Mater. Chem. A* **2017**, *5*, 2539–2549. [[CrossRef](#)]
115. Han, C.; Liu, F.; Liu, J.; Li, Q.; Meng, J.; Shao, B.; He, Q.; Wang, X.; Liu, Z.; Mai, L. Facile template-free synthesis of uniform carbon-confined V₂O₃ hollow spheres for stable and fast lithium storage. *J. Mater. Chem. A* **2018**, *6*, 6220–6224. [[CrossRef](#)]
116. Liu, T.; Zhang, L.; Cheng, B.; Yu, J. Hollow Carbon Spheres and Their Hybrid Nanomaterials in Electrochemical Energy Storage. *Adv. Energy Mater.* **2019**, *9*, 1803900. [[CrossRef](#)]



© 2020 by the authors. Licensee MDPI, Basel, Switzerland. This article is an open access article distributed under the terms and conditions of the Creative Commons Attribution (CC BY) license (<http://creativecommons.org/licenses/by/4.0/>).